Post-eruption evolution of maar lakes and potential instability: The Lake Pavin case study, French Massif Central

Jean-Claude Thouret, P. Boivin, D. Miallier, F. Donnadieu, J.-P. Dumoulin, P. Labazuy

Post-eruption evolution of maar lakes and potential instability: The Lake Pavin case study, French Massif Central

J.-C. Thouret[a], P. Boivin[a], D. Miallier[b], F. Donnadieu[a], J.-P. Dumoulin[c], P. Labazuy[a]

[a] *Université Clermont-Auvergne, Laboratoire Magmas et Volcans LMV, CNRS, OPGC et IRD, Campus Les Cézeaux, 6 avenue Blaise Pascal, 63178 Aubière, France*
[b] *Université Clermont-Auvergne, Laboratoire de Physique de Clermont LPC, CNRS, IN2P3, Campus Les Cézeaux, 4 avenue Blaise Pascal, 63178 Aubière, France*
[c] *Laboratoire des Sciences du Climat et de l'Environnement, LMC14, Bâtiment 714, CEA-Orme des Merisiers, F-91191 Gif-sur-Yvette Cedex, France*

Few studies have focused on the post-eruption evolution of maar craters and associated lake level changes, although breaching of the crater rim poses mass-flow and flood hazards long after the initial eruption. Lake Pavin is a maar lake in the French Massif central formed by an eruption c. 6700 years ago. The maar is perched on the edge of a glacially-shaped valley and the rim overlooks the surrounding subdued landscape. The rim is breached to the north by an overflow channel, and to the south the maar has cut into the flank of the Montchal scoria cone and lava flows. Incision of the lake outlet led to the growth of an alluvial fan that pushed the Couze Pavin River towards the north side of the Gelat valley.

Two lake terraces within the crater are used to determine stages in the evolution of the lake. The highstand Stage 1 terrace +18 m above the current lake level indicates that the post-eruption lake surface and volume was 15% and 38% larger than the present-day lake, respectively, prior to the 5-7th Century CE. The poorly preserved Stage 2 bench, +4.35 m on the west side of the natural dam, indicates that incision paused between Stage 1 and achievement of present lake level (Stage 3) before the 18th Century. Four units of streamflow deposits (c. 0.087 km^2 in area and 0.14–0.18 km^3 in volume) that formed the fan at the mouth of the outlet in the Gelat valley have been ^{14}C dated to between the 9th and 16th Century. From the fan sedimentology, we infer that the lake level dropped slowly between highstand Stages 1 and 2, when the outlet cut down through the rim saddle. The lake level drop accelerated between Stage 2 and Stage 3 before the 14th Century, inducing small debris flows. The latter may have resulted from heavy rainstorms, but there is no evidence for catastrophic events. Stepwise downcutting of the north rim saddle was also governed by contrasted properties of the deposits forming the dam. The current lake level has been stable since at least the early 18th Century, but the long-term stability of the dam is at risk.

1. Introduction

Maars represent the second most common terrestrial volcanic landform after cinder cones and, together with tuff rings and tuff cones, the most common monogenetic volcanoes formed by explosive, phreatomagmatic eruptions (Ollier, 1967; Lorenz, 1973, 1986, 2003; White and Ross, 2011; Martin et al., 2007; Németh et al., 2011; de Silva and Lindsay, 2015; Valentine et al., 2017). A maar is a broad, shallow, subcircular volcanic crater with sides cut into the country rocks. Maar craters are surrounded by low rims of tephra-ring deposits, composed of a mixture of ejecta from subsurface explosions, resulting from the interaction of magma, gas and groundwater (Lorenz, 2003; Graettinger and Valentine, 2017). The inner tephra deposits dip at about 33° towards the crater, but the outer deposits dip outward at 5–10°. Slopes angles depend on volume ejected, the pre-eruptive topography, and the moisture content of the tephra (Lorenz, 2003).

Maars usually have simple eruptive histories (Palladino et al., 2015). They usually result from a series of short-lived (hours to a few days) explosive events together with annular collapses. Studies of maar deposits and laboratory experiments sought to understand how powerful the magma-water interactions create wide and relatively deep craters (Wohletz, 1986; Németh et al., 2008; White and Ross, 2011; Valentine and White, 2012; Németh and Kereszturi, 2015; Graettinger and Valentine, 2017; Valentine et al., 2017). Subsequent volcanism is limited to late eruptive phases at the vent and deposition of tephra from neighbouring volcanoes (Lorenz, 2007). Scoria cones are often created immediately after the maar explosions (e.g., the Chaîne des Puys; Boivin et al., 2017), and lava flows from cones are sometimes trapped

E-mail addresses: j-claude.thouret@uca.fr (J.-C. Thouret), Boivin@opgc.univ-bpclermont.fr (P. Boivin), didier.miallier@clermont.in2p3.fr (D. Miallier), Franck.Donnadieu@uca.fr (F. Donnadieu), Jean-Pascal.Dumoulin@lsce.ipsl.fr (J.-P. Dumoulin), P.Labazuy@opgc.fr (P. Labazuy).

in maars (e.g., Aranda Gomez et al., 1992; Boivin and Mergoil, 1993; Martin and Németh, 2007). After the formation of the Pavin maar no further volcanic activity took place.

Here we focus on the post-eruption evolution of the Lake Pavin maar. Pavin (45°55′N, 2°54′E), the youngest volcano in continental France, erupted 6730 ± 130 years ago, 33 km south of the Chaîne des Puys on the east slope of the Monts-Dore and Sancy volcano in the French Massif central (Fig. 1). Pavin was the last among a group of four cones and maars, all within 1–4 km distance and formed within a time interval of five centuries (Camus et al., 1973; Boivin et al., 2012, 2017; Boivin and Thouret, 2014; Juvigné and Miallier, 2016). Lake Pavin is a circular (770 m in diameter) and 92 m-deep lake 0.445 km^2 in area (Table 1). It is isolated from the surrounding landscape by a ring 40 to 70 m high (6 to 15 m-thick tuff deposit on >30 m-thick reamed out lava-flow cliffs) (Figs. 1, 2; Thouret et al., 2016). The high rim is related to the composition and eruptive style (Boivin et al.,

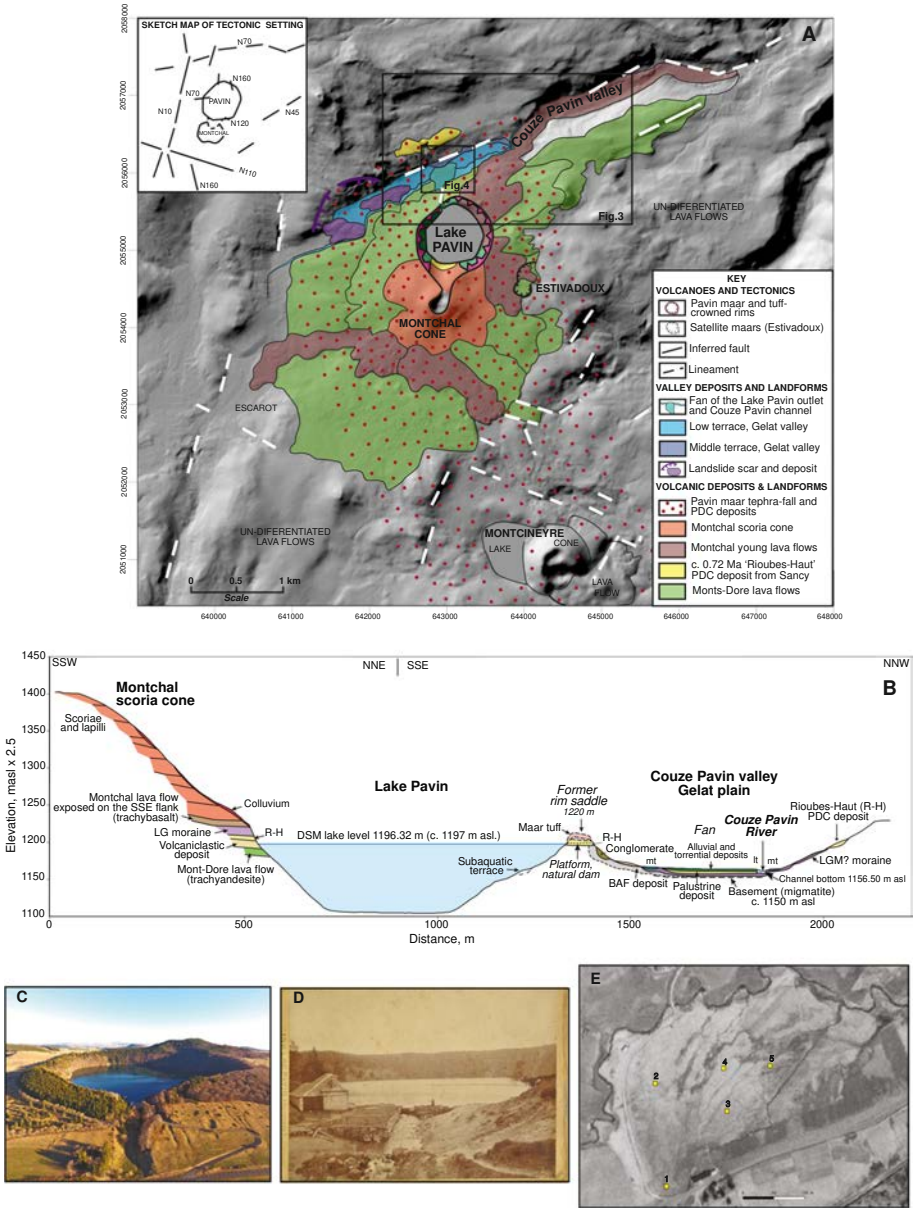

Fig. 1. A. Geological setting of the Pavin maar and Gelat valley (after Thouret et al., 2016, revised). **B**. South-North cross section from Montchal cone, Lake Pavin to the Couze Pavin–Gelat valley; 'mt' stands for middle terrace, 'lt' low terrace, LGM Late Glacial Maximum, LG Late Glacial (see Fig. 4). Subaquatic terrace c. 40 m below the lake level refers to Henriet (2009) and Chapron (2010, 2012), see Discussion, Section 6. The dashed black line pinpointed by an arrow 'platform and natural dam' indicates the present-day profile across the septum between the lake and the headwall of the outlet gorge. The geometry of the formations and deposits has been extrapolated due to poorly exposed outcrops in forest areas and to rapid variations in thickness and extension locally. Thickness of deposits in the Couze Pavin-Gelat valley and across the north rim of the maar has been exaggerated for the purpose of readability. **C**. Low angle air photograph (F. Lécuyer courtesy) looking south, showing the steep and narrow outlet gorge to the north and the perched Lake Pavin maar with respect to the Couze Pavin (Gelat plain) valley. The large platform at the northern entrance of the lake providing access for tourists coincides with the notch and the saddle at the originally lowest north rim. The prominent rim overlooks the subdued, volcanic and glacially shaped landforms except for the Montchal cone. **D**. The regulated lake outlet between 1870 and 1890 (Photograph by Sanitas, courtesy of P. Chatelus). Note the excavated lake outflow channel about 1 m deep and 15 m long, with a metal gate (fisherman for scale), and the c. 4.35 m-high preserved bank on the right handside. This was the stillstand lake stage 2 at c. 1201 m asl. **E**. National Geographical Institute (IGN) aerial photograph of 1955 showing the Gelat plain and the Couze Pavin, the channel of which was pushed north by the growth of the fan. Levees (berms) separated by rills (wet channels) formed a fan from the mouth of the outlet (near the building at the lower edge) towards the north and NE. Yellow rectangles indicate the trenches 1 to 5 dug during this project. The lake outlet feeds a rectilinear stream to the east. The marsh of the easternmost fan area is drained by a small tributary to the Couze Pavin. See Fig. 4 for detailed mapping of the fan and Fig. 7 for stratigraphy.

2012, 2017). Trachytic and basaltic maars exhibit similar landforms, but explosivity depends on the volatile content of their magmas (Boivin and Thouret, 2014). The Pavin maar tuff is trachyandesitic (benmoreite) in composition, much less common than basaltic and trachybasaltic maars. Pavin's eruption was probably highly explosive because of the magmatic volatile content of benmoreitic lavas (Villemant et al., 2016; Rondet et al., 2019). Tephra fall from high columns was dispersed southward, and the 1-cm isopach lies 14.5 km away from the crater (Leyrit et al., 2016). In addition to phreatomagmatic products, Pavin deposits include pumice-fall beds depleted in phreatomagmatic components and attributed to a Plinian stage intercalated in the maar eruption (Boivin et al., 2012). Pyroclastic current deposits spread out around the crater, filling pre-existing valleys, and smoothed out slopes as far as 2 km from Pavin.

1.1. Scope: post-eruption evolution of maars and lakes

Some post-eruption evolution of maars has been described through the analysis of crater infilling sediments (Fox et al., 2015; Kaulfuss, 2017; Fepuleai et al., 2018). Other studies depict the initial crater rim erosion and shallow lake impoundment immediately after the eruption (e.g., Pirrung et al., 2007). Few maar-forming historical eruptions have been documented, which renders the post-eruption evolution difficult to assess. The most recent ones are the Nilahue maar, Rininahue, Chile in 1955 (Müller and Veyl, 1957; Illies, 1959), Iwo Jima, Japan in 1957 (Corwin and Forster, 1959), the Ukinrek maars, Alaska in 1977 (Kienle et al., 1980; Self et al., 1980; Büchel and Lorenz, 1993; Ort et al., 2018), and the Westdahl maar on the Aleutian Islands in 1978 (Wood and Kienle, 1990). The Ukinrek West Maar formed within 3 days; its final crater was 175 m wide and 35 m deep. The East Maar was created in the following 8 days and reached a diameter of 340 m and a depth of 70 m after its syneruptive growth. A limited number of studies also describe the evolution of maars and tuff rings within days to years following the explosive events. These include maars formed by the Miyakejima 1983 eruption (Aramaki et al., 1986), Ukinrek maars formed in 1977 in Alaska (Büchel and Lorenz, 1993; Ort et al., 2018) and a shallow maar surrounded by a tuff ring created in 1913 in Ambrym, Vanuatu, studied by Németh and Cronin (2007) 94 years later.

Maar craters commonly intersect the water table and the craters fill with water, creating crater lakes (Delmelle and Bernard, 2000; Christenson et al., 2015). Maar lakes abound in monogenetic fields like Eiffel (Germany), Chaîne des Puys and Velay (France), Newer Volcanic Province (Australia), Jeju Island (South Korea), Seward peninsula (Alaska), the Auckland field (New Zealand) and many more. At least 474 volcanoes (not only maars) host crater lakes according to Pasternak and Varekamp (1997) and the VOLADA database (https://vhub.org/tags/voladadatabase). Volcanic lakes have been the focus of recent multidisciplinary studies summarized by Delmelle and Bernard (2000), Varekamp et al. (2000), Delmelle et al. (2015), and developed by Rouwet et al. (2015). Evidence from historical maars suggests that craters fill with water shortly after eruptions (White and Ross, 2011). For instance, a shallow lake formed within one or two weeks following the eruption of the Ukinrek West and East maars (Alaska), between 30 March and 9 April 1977 (Pirrung et al., 2007), but the lake in the East maar rose to a stable level 60 m higher than the May 1977 level only around August 1990. The permeable roots of maars and the excavation of their craters below the pre-eruptive surface give them a direct hydraulic connection with the groundwater system, so maars experience lacustrine conditions early in their development (Fepuleai et al., 2018).

1.2. Hazards around maars and meromictic lakes

Maar lakes and their rims may become hazards for people visiting the area and settlements in the vicinity (Lorenz, 2007). Documented lake gas outbursts and overflows have been untangled from myths and legends at Lake Albano (e.g., de Benedetti et al., 2008; Rouwet et al., 2019). Lake Albano maar is the most recent eruptive centre of Colli Albani volcano a few kilometers SE of Rome, Italy. At Lake Pavin, despite recent publications dealing with sedimentology, limnology, biogeochemistry, and chronology (Sime-Ngando et al., 2016; Chassiot et al., 2018), the so-called Lake Pavin misbehaviour (Meybeck, 2016a, 2016b) has not been well documented or understood.

Lake outlets are tributaries to major rivers running through populated areas down valley, so lake overspills and mass flows pose potential hazards to people living downstream of the maars. This is particularly the case of meromictic lakes in relatively deep maars. Meromicticity defines lakes that have layers of water superimposed and geochemically different water bodies that do not intermix (Jézéquel et al., 2008; Rouwet et al., 2015). Meromictic lake overturns and limnic eruptions that trigger gas outbursts and release water represent significant threats (Delmelle et al., 2015; Kusukabe, 2017). For example, Alvarado et al. (2011) described several lake overturns in recent years at the Laguna Hule and Rio Cuarto maars, Costa Rica. Maar crater lakes, particularly the meromictic category, are widely known for their dissolved gas content. Lakes Monoun and Nyos in Cameroon became famous in the wake of the gas disasters in 1984 and 1986 (Kusukabe, 2017). The August 1986 Nyos event led to the death by asphyxiation of at least 1700 people and 3000 livestock (Kling et al., 1987). Other CO_2-and/or CH_4-rich volcanic lakes in the world include Laacher See (Germany) (Aeschbach-Hertig et al., 1996), Lake Van (Turkey) (Kipfer et al., 1994), Lake Albano and the two Monticchio Lakes (Italy) (Anzidei et al., 2007; Caracausi et al., 2013), Laguna Hule and Rio Cuarto (Costa Rica) (Alvarado et al., 2011), and Lake Pavin (France) (Camus et al., 1993; Henriet, 2009; Aeschbach-Hertig et al., 2002; Jézéquel et al., 2008; Olive and Boulègue, 2004; Gal and Gadalia, 2011). Pavin is the only meromictic lake in France (Jézéquel et al., 2008), arising from the unusual lake depth ratio as a result of the funnel-shaped crater inside a high-relief maar ring (Table 1, Figs. 2, 3; Sime-Ngando et al., 2016; Thouret et al., 2016).

As sudden lake overturns and lethal gas outbursts occurred in Cameroon at Lake Nyos in 1986 (Kling et al., 1987; Lockwood et al., 1988; Tassi and Rouwet, 2014) and Lake Monoun two years earlier (Kling et al., 2005; Kusukabe, 2017), new investigations considered the volcanic lakes in Auvergne, and Pavin in particular, in the early 1990's. The monimolimnion contains substantial amounts of CO_2 and CH_4. A mineral sub-lake spring at −65 m emits CO_2 whose carbon magmatic isotope ratios indicate a source in the upper mantle (Alberic et al., 2013). However, the high CO_2 solubility yields a weak (3.3 bars) partial pressure against the high (9.88 bars) hydrostatic pressure at the 92 m-deep lake bottom. Camus et al. (1993), Aeschbach-Hertig et al. (2002), Olive and Boulègue (2004) and Jézéquel et al. (2011) all concluded that Lake Pavin did not present an imminent threat.

1.3. Maar lake level fluctuations and formation of overflow channels

Besides meromicticity, slow lake leakage may lead to the release of a large volume of water without any external factors (e.g., earthquakes and wave oscillations known as seiches). In newly formed maars, the lake level rises until an equilibrium is reached between the rates of incoming and outgoing water. Sources of water loss may include evaporation, subsurface seepage, and overflow when the lake level reaches the lowest point on the crater rim. At such a location, the upper portion of the lake is contained only by its adjacent natural pyroclastic dam; continued leakage through or surface outflow across the dam can erode, lowering lake level until a new equilibrium of water flow, erosion, and rock resistance is established. If the saddle erodes rapidly or fails catastrophically, the event produces break-out floods. From the review of literature by Manville (2015), the occurrence of break-out floods is relatively common worldwide with decreasing resistance of natural dams or increasing surface outflow induced by precipitation change over time. Newly created volcanic lakes are particularly vulnerable to breaching due to the inherent instability of their dams, which are

Table 1
Geometric and morphometric characteristics of the Lake Pavin, selected Auvergne maars, other maars known for lake overbank floods or lake outbursts, and comparison with statistical parameters from the maar VLS worldwide dataset after Graettinger (2018).

Maar name, location, centre coordinates, elevation m asl	Rim diameter (km) Catchment area (km^2)	Eruption Age (yr); Overflow, BCE	Mean and maximum rim height, m	Rim height/diameter ratio	Excavation depth (m): mean, maximum	Depth diameter ratio; DepthRatio[b] (V/S)/D_{major}	Aspect ratio *AR* $D_{minor}/D_{major,m}$	Elongation *EL* $A/\pi(D_{maj}/2)^2$	Isoperimetric circularity *IC* $4\pi A/P^2$	Surface *S* km^2 Volume $V10^6$ m^3	Mean/Ma × slope bedding dip (°)	References
Pavin maar, Auvergne France	Mean 0.905 Max 0.931	6730 ± 170= 4720 ± 170 BCE	Mean 40 Max 70	0.044 0.077	Mean 90 Max 146	Mean 0.099 Max 0.156	dm 880/DM 931 = 0.945	644,683/540,786 =0.940	8,097,218,5/$(2900)^2$ =0.962	S 0.644	Inner slopes 30–45° Outer slopes 10–25°	Thouret et al., 2016; from Graettinger database 2018
Pavin maar without Montchal cone	Mean 0.971 Max 0.975	6730 ± 170= 4720 ± 170 BCE	Mean 58 Max 110	0.060 0.112	164 without 14 m-thick infill sediment	Mean 0.168 Max 0.168	Dm 967 DM 975= 0.992	691,000/ 639,866 =0.926	8,678,960/ $(3034)^2$ =0.943	S 0.691	Inner 30–45° Outer 10–25°	Boivin, this study; Juvigné and Miallier, 2016
Pavin maar with Montchal open South flank	Mean 1079.5 Max 1206	6730 ± 170= 4720 ± 170 BCE	Mean 70 Max 167	0.064 0.138	176 without 14 m-thick infill sediment	Mean 0.146 Max 0.145	Dm 953 DM 1206= 0.790	754,000/ 1,142,314 =0.660	9,470,240/ $(3374)^2$ =0.832	S 0.754	Deposits >35° Pavin 15–25% Montchal	Boivin, this study
Lake Pavin, meromictic, 45°29′ 44″N, 2°53′17″ E, 1197 m	Mean 0.770 Max 0.775 0.81 km^2	6730 ± 170= 4720 ± 170 BCE		0.05 0.06	Mean 92 Max 116, without sediment infill	Mean 0.118 Max 0.149 DR 0.069	dm 763.1/DM775 = 0.981	451,000/ 474,688 =0.951	5,666,364/ $(2594)^2$ = 0.843	S 0.449 V 23.70	Deposits ≥35° in lake, 20–25° above	This study
Chauvet maar, Auvergne, France	Mean 0.950 Max 1100	>10,000?	Mean 25 Max 50	0.026 0.045	Mean 62 Max 65	Mean 0.06 Max 0.059	dm 900/DM 1100 = 0.818	708,462/ 949,850 = 0.746	8,901,117/ $(2984)^2$ =0.999	S 0.709	Inner 30–45° Outer 10–25°	Juvigné, 1992; Chapron et al., 2012; This study
Lake Chauvet 45°27′35″ N, 2° 49′52″ E, 1162 m	Mean 0.840 Max 0.860 1.2 km^2	>10,000?		0.03 0.06	Mean 63 max 86, without sediment infill	Mean 0.075 max 0.10 DR 0.030	dm 730/DM 860 = 0.849	550,000/ 580,586= 0.948	6,910,200/ $(2639)^2$ =0.992	S 0.555 V 17.30	Deposits ≥35° in lake, 20–25° above	Chassiot et al., 2016b; Chapron et al., 2012; Meybeck et al., 1975

Godivelle d'En-Haut, Auvergne 45°23′14″ N, 2° 55′01″E, 1239 m	Mean 0.430 Max 0.492 0.28 km^2	Late Glacial/LGM	Mean 21 Max 30	0.049 0.061	Mean 30 Max 44	Mean 0.070 Max 0.090 DR 0.021	dm 368/ DM 492 = 0.748	146,000/ 173,407= 0.842	1,833,760/ $(1401)^2$ =0.934	S 0.146 V 2.74	Inner >30° Outer 15°	Juvigné, 1992; Meybeck et al., 1975; This study
Lake Nyos, NW Cameroon, 06° 26′17″N, 10°17 54″E, 1091 m	Mean 1870 Max 2000 8 km^2	c.400? 8750± 490[c]	Mean 40 Max 70	0.021 0.035	Mean 95 Max 210	Mean 0.05 Max 0.105 DR 0.033	dm 1200/DM 2000 = 0.600	2,750,000/ 3,140,000 = 0.875	34,551,000/$(5874)^2$ =1.00	S 2.75 V 180	Inner: steep Outer: gentle	Lockwood and Rubin, 1989; Kusukabe, 2017; Tanyileke et al., 2019; Tchindjang, 2018
Meromictic lake Monoun, W Cameroon, 05°34′44″N,10° 35′03″E, 1081 m	Mean 0.822 Max 1600 21.3 km^2	Unknown Age Overflow 1984	Mean 10 Max 30	0.012 0.018	Mean 90 Max 99	Mean 0.109 Max 0.062 DR 0.019	Dm 411/ DM 1600 = 0.437	530,000/ 2,009,600= 0.263	6,658,920/ $(2581)^2$ =0.999	S 0.53 V 15.7	Inner: steep Outer: very gentle	Kusukabe, 2017; Tanyileke et al., 2019
Lake Albano, Colli Albani, Italy, 41°44′ 06″ N, 12°41′11″E 292 m	Mean 1410 Max 3280 16.6 km^2	36,000 to 8000 Lahar:5800 Overflow: 398 BCE	Mean 150 Max 250	0.106 0.076	Mean 160 Max 167.5	Mean 0.113 Max 0.051 DR 0.022	Dm 1300/DM 3280= 0.396	6,200,000/ 8,445,344 =0.734	77,896,800/$(8858)^2$ =0.992	S 6.20 V 447.5	Inner slopes Outer slopes	Anzidei et al., 2007; Funiciello et al., 2003; De Benedetti et al., 2008
Lake Monticchio Grande, Mt. Vulture, 40°55′ 52″N, 15°36′15″E, Italy, 655 m	Mean 0.742 Max 0.850 4 km^2	140,000; Gas outbursts 1770 CE, 1810	Mean 10 Max 25	0.014 0.030	Mean 30 Max 35	Mean 0.040 Max 0.041 DR 0.011	Dm 590/ DM 850 = 0.695	430,000/ 567,163 = 0.759	5,402,520/ $(2331)^2$ =0.994	S 0.43 V 3.98	Inner slopes Outer slopes	Cioni et al., 2006; Caracausi et al., 2013; Cabassi et al., 2013
Lake Monticchio Piccolo, Mt. Vulture, 40°55′ 58 N, 15°36′46 E, Italy, 659 m	Mean 0.370 Max 0.490 1.7 km^2 Meromictic	140,000; Gas outbursts 1820 CE	Mean 5 Max 10	0.014 0.021	Mean 35 Max 37	Mean 0.095 Max 0.076 DR 0.039	Dm 320/ DM 490= 0.654	170,000/ 188,479= 0.902	2,135,880/ $(1540)^2$ =0.902	S 0.17 V 3.25	Inner slopes Outer slopes	Spicciarelli and Marchetto, 2019; Cabassi et al., 2013
Maar VLS[a]	1.122 ± 0.833		10–150	0.009–0.13	5–400	Average 0.10	0.81 ± 0.13	0.80 ± 0.12	0.90 ± 0.08			Graettinger, 2018
Mode	0.603						0.84	0.62	0.93			
50th percentile	0.805						0.83	0.82	0.92			

[a] Maar Volcano Location and Shape (Maar VLS).
[b] DR Depth Ratio as proposed by Rouwet et al. (2019).
[c] See discussion on the Lake Nyos age in Kusukabe (2017), reporting the 226Ra-230Th age from Aka and Yokoyama (2013).

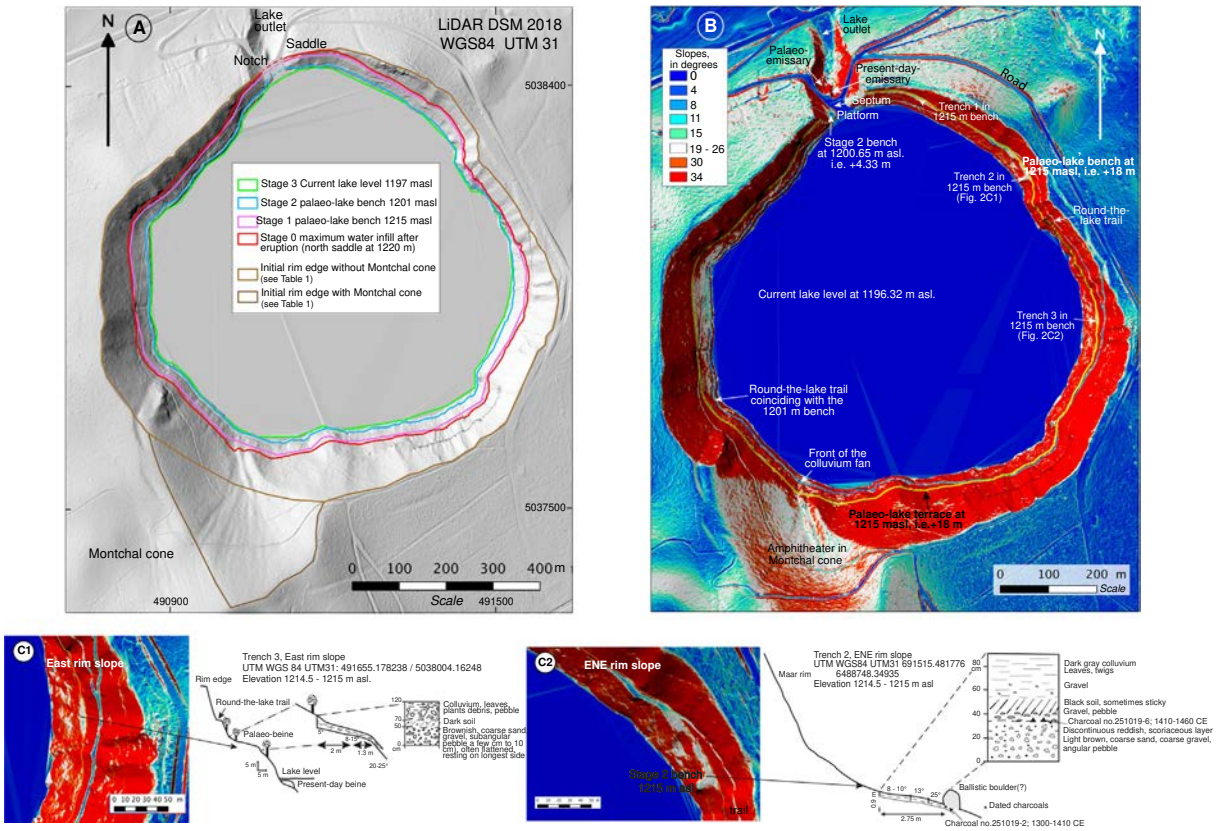

Fig. 2. A. LiDAR-derived DSM showing how the slope system and a narrow bench landform suggest the location of a beine (lake terrace) at 1215 m asl, i.e., +18 m above the current lake level at c. 1197 m asl. The LiDAR data was acquired by SETIS, delivered to CRAIG, and co-funded by the European Fund for Regional Development. **B.** LiDAR DSM of the maar indicating the initial rim top (Stage 0) with and without the neighbouring Montchal cone to the south, the lake bench of Stage 1 at 1215 m, the preserved bench at c. 1201 m suggesting Stage 2, and the green line indicating the current lake level. Contour line colours are as in Figs. 5 and 11. **C**. Enlarged segment of the lake bench at 1215 m asl on the east (1) and SE (2) rim inner slopes showing the slope angles and trenches dug in the surficial deposits. The positions of ^{14}C dated charcoal are indicated.

typically made up of unconsolidated, low density material, and without the benefit of engineered spillways. Some lake overflows have been prevented by human intervention, such as the Roman tunnel that artificially dropped the rising Lake Albano level in 398 BCE (Funiciello et al., 2003; de Benedetti et al., 2008), and tunnels successively dug through the lava damming Lake Kelut in 1923–1926 to artificially lower the level following the devastating 1919 eruption (Suryo and Clarke, 1985). In contrast, a very small number of dam failures have been described at maars (e.g., Manville, 2015), in contrast to crater lakes on volcanoes (e.g., Ruapehu Crater Lake: Schaefer et al., 2018) and numerous intracaldera-lake break-out cases (Manville, 2010, 2015).

1.4. Rationale and objectives of the Lake Pavin case study

Lavina and Del Rosso d'Hers (2008, 2009) postulated early Middle Age eruptive activity and a catastrophic flood triggered by lake breakout subsequent to subaquatic landslides in Lake Pavin. The authors and Del Rosso-D'Hers et al. (2009) observed deposits along the Couze Pavin channel north and NE of the maar, and claimed they were deposits of a flood that wreaked havoc around 800 CE in La Villetour, a suburb of the town of Besse 3.5 km down valley. A BRGM report (2007) has already challenged these findings. This claim originated from geologic mapping of the area by both authors, following numerous earlier studies on volcanic lakes in Auvergne, and Lake Pavin in particular (e.g., Lecoq, 1835; Boule, 1896; Bruyant, 1909; Glangeaud, 1916; Eusébio and Reynouard, 1926; Omaly, 1968; Aeschbach-Hertig et al., 2002). The flood was arbitrarily linked to sedimentological and chronological data on subaquatic landslide deposits, first detected by geophysical methods near the NE Lake Pavin shoreline (Henriet, 2009).

Following the claim, geological and geotechnical studies have increased at Lake Pavin, including studies of the mechanical characteristics of the deposits forming the rim, and measurements of fractured lava cliffs around the maar (BRGM, 2007, 2009, 2011). Geomorphological and geological maps depicted a variety of mass movements, gullies and runoff acting on the rim slopes (Thouret et al., 2016). Sedimentologists led by Chapron et al. (2010, 2012), followed by Chassiot et al. (2016a, 2016b, 2016c, 2018) have summarized natural hazards associated with a group of lakes in the French Massif Central, particularly the Pavin and neighbouring Chauvet maar lakes. Geophysical investigations, sedimentary cores and ^{14}C ages have allowed the authors to propose that subaquatic mass movements displaced unconsolidated sediment on the steep (>33°) inner slopes of the maar lake. According to these authors, 'catastrophic' mass movements occurred twice, between 580 and 640 CE (later rounded to 600) and as recently as between 1260 and 1300 CE (later rounded to 1300).

The objectives of the present paper are threefold: (1) To describe the Gelat outwash fan deposits, and so understand how the fan was formed; (2) To quantify post-eruption erosional processes acting on the rim; (3) To map the Lake Pavin rim, outlet gorge, and the adjacent Couze Pavin valley to obtain clues on rim and natural dam instability.

2. Materials and methods

Several methods and tools have been exploited to analyze the Lake Pavin evolution.

1. Geological and geomorphological mapping has used the Napoleonian cadaster (1828), and the French ordnance survey map (1:80,000 scale, 1835–1845) that display the Couze Pavin river

diverted by the Gelat fan (Figs. 1 to 4). We have exploited PhD theses achieved in the area (Bourdier, 1980; Lavina, 1985), a draft of the unpublished 1:50,000 scale geological map of Besse, and reports on the maar rim hazards presented by BRGM (2007, 2009, 2011). Considerable progress in mapping, however, was achieved in 2016 with the drone-based DEM and in 2018 with the Laser light detection and ranging (LiDAR) digital surface model (DSM, Fig. 2; ESD Fig. 1). The LiDAR DSM represents an advance on the drone-based DEM used to map the area in 2016 (Thouret et al., 2016) because it has enabled us to look through the forest cover and detect landforms on the maar rim, the outlet and the lowermost reach of the Couze Pavin valley. Figs. 2 to 5 exhibit maps and cross sections based on the DSM.

2. The LiDAR DSM also helps derive morphometric indices. Table 1 displays the geometry and morphometry of Lake Pavin and other meromictic maar lakes according to indices proposed by Graettinger (2018) and others, e.g., depth ratio (Rouwet et al., 2019). We propose another morphometric index, the perched maar index (PMI), to account for high-relief maar rims located above, and deep lakes adjacent to, the local drainage baseline, which favour the outlet headward erosion and threaten the stability of natural lake dams.
3. Field investigations, stratigraphy and ^{14}C chronology have been combined to study the landforms (Figs. 2, 3, 6; Table 2). We dug three trenches in the highstand lake bench on the rim slopes and five

Table 2
Chronological dataset for this study based on ^{14}C ages from LMC14, Gif-sur-Yvette, France (ARTEMIS AMS facility), obtained around the Lake Pavin maar: Gelat valley in fan, alluvial and marsh deposits, maar dam in rim deposits, high lake terrace on the east maar slope (see references for Figure numbers and location of sites). Projection system Lambert WGS 84/UTM Zone 31 EPSG 32631. Calibration using Intcal 2013, computation using the chronomodel software. Symbol meaning: # Dubious date in the stratigraphic context of the Unit1. The gyttja sample has likely been mixed with recent small roots.

Laboratory SacA no., Figure, site	Sampling site, sample number (no.)	UTM coordinates Elevation, m	Unit/Layer depth (m)	Dated material	mg C	pMC and error pMC	^{14}C date year BP	Age Cal BP (Intcal 2013)	Calibrated dates CE/BCE	Comment
SacA 59399 Fig. 5, site 1	East rim, trench, paleo-beine, no. PAV251019-2	691,515.4 6,488,748.3 1214.5	Layer 2, 0.40–0.45	Charcoal	1.63	94.323 ± 0.24	470 ± 30	540–490 (95.1%)	1410–1460 (95.1%)	Charcoal top organic soil above gravel layer 3. 15th century
SacA 59400 Fig. 5, site 2	East rim, trench, paleo-beine, no. PAV251019-6	691,515.4 6,488,748.3 1214.5	Layer 3 0.65	Charcoal	1.70	92.946 ± 0.231	590 ± 30	650–580 (67.8%) 570–540 (27.4%)	1300–1370 (67.8%) 1380–1410 (27.4%)	Charcoal above gravel layer3 on paleo-terrace. 14–15th century
SacA 57676 Fig. 3, site 3	Gelat fan, TR2, Unit 5, no. PB18-08-11-04	691,038.1 6,489,262.4 1163.50	Unit 5, 0.40–0.50	Base of soil	1.19	96.944 ± 0.52	250 ± 30	320–270 (56.7%) 170–150 (19.7%) 430–380 (14.6%)	1630–1680 (56.7%) 1780–1800 (19.7%) 1520–1570 (14.6%)	Minimum age above cobble-rich unit 4: 16–18th century
SacA 53940 Fig. 3, site 4	Gelat fan, TR4, Unit 5	691,148.8 6,489,286.4 1160.75	Unit 5 0.20–0.30	Top soil	1.15	105.4570 ± 0.28854	−425 ± 30	c.0	1956–1957 or 2007–2009	Minimum age above unit 4: 20th century
SacA 51053 Fig. 3, site 5	Gelat Fan TR3, Unit 1, gyttja no.1	691,154 648,922.3 1162.71	Unit 1 2.65	Gyttja	1.14	85.35476 ± 0.23229	1270 ± 30	1290–1170 (92.3%)	660–780 (92.3%)	7–8th century
SacA 51054 Fig. 3, site 6	Gelat Fan TR3, Unit 2, gyttja no.2	691,154 648,922.3 1162.71	Unit 1 2.85	Gyttja	1.00	85.78429 ± 0.24310	1230 ± 30	1190–1070 (62.7%) 1260–1200 (32.5%)	760–880 (62.7%) 690–750 (32.5%)	7–9th century
SacA 53936 Fig. 3, site 7	Gelat East fan Hand auger, W outlet side Unit 2,core no. S203	0491332 5,038,835 1157	Unit 2 1.00–1.10	Wood fragment	1.20	85.074 ± 0.233	1300 ± 30	1290–1220 (64.3%) 1210–1180 (30.8%)	660–730 (64.3%) 740–770 (30.8%)	7–8th century
SacA 57677 Fig. 3, site 8	Gelat East fan, Stream bank facing NW, Unit 1, no. S304	0491283 5,038,845 1158	Unit 2 0.90–1.08	Gyttja Beneath sand layer	1.47	82.828 ± 0.227	1515 ± 30	1420–1340 (68.8%) 1520–1460 (24.4%)	530–610 (68.8%) 430–490 (24.4%)	5th–7th century
SacA 51055 Fig. 3, site 9	Gelat Fan, TR5, Unit 1, gyttja no.3	92,617 39,983 1160.25	Unit 1, 1.55–1.60	Gyttja	0.95	97.14549 ± 0.24568	235 ± 30 #	320–270 (50%) 190–150 (33%) c. 10 (7%)	1630–1680 (50%); 1760–1800 (33%); c. 1940 (7%)	# Dubious age; recent roots mixed with gyttja?
SacA 51056 Fig. 3, site 10	Gelat Fan, TR5, Unit 1, gyttja no.4	691,223.3 6,489,291.5 1160.25	Unit 1, 1.65–1.70	Gyttja	1.44	82.29632 ± 0.22188	1565 ± 30	1530–1390 (95%)	420–560 (95%)	5th–6th century
SacA 51057 Fig. 3, site 11	Gelat Fan, TR5 Unit 1, Hand auger, gyttja no.5	691,223.3 6,489,291.5 1160.25	Unit 1, 1.75–1.85	Peat	1.59	82.42605 ± 0.22628	1555 ± 30	1530–1380 (95%)	420–570 (95%)	5th–6th century
SacA 46776 Fig. 3, site 12	Couze Pavin Bank, fan front stream, no. PB09–0205-3	491,229 5,038,965 1160	Unit 3 0.70–0.90	Micro-charcoals in grey clay soil	1.48	72.97917 ± 0.22930	2530 ± 30	2740–2680 (35.8%) 2640–2610 (13.7%) 2600–2490 (45.5%)	−790 to −730 (BCE) (35.8%) −690 to −660 (BCE) (13.7%) −650 to −540 (BCE) (45.5%)	Organic soil preceding the fan formation: 6 to 8th century BCE
SacA 52019 Fig. 4, site 13	Maar rim upper E slope, Restaurant, no. PB17-1031-4bis/C1057	491,151.42 5,038,479.1 1200	Layer 4 1.40–1.45 below section top	Micro-charcoals in paleosol	1.43	39.81094 ± 0.19021	7400 ± 40	8150–8350 (95%)	−6400 to −6200 (BCE) (95%)	Prior to the maar eruption c. 6700 years ago, and un-related to palaeolakes

deep trenches into the fan deposits and several sections along the Couze Pavin banks (Figs. 1E, 3, 4). Sections cut on both slopes of the maar notch and along the outlet gorge led us to revise the stratigraphy of the Monts-Dore–Sancy deposits that underlie the rim tuff deposit and form the dam impounding Lake Pavin.

4. Laboratory analyses determined the sedimentology, lithology, and composition of the fan and maar deposits. From the five trenches dug in the fan (Figs. 4, 7A, B), 25 samples have been sieved for grain size distribution, while pebble- to sand-sized fractions have been sorted out for lithological components. We assigned the source of rock samples, either to the Pavin maar and Montchal cone catchment, the Monts-Dore–Sancy lavas, or other formations found in the Couze Pavin watershed.
5. Electrical resistivity tomography (ERT) and ground-penetrating radar (GPR: see method, ESD text) allowed us to map the geometry of fan deposits, to determine the contact between the valley deposits and the basement, and to distinguish the sub-surface valley-filling deposits (Fig. 8; ESD Fig. 2A). A 240 m-long survey was acquired in the N-S direction (N008°) with an electrode spacing of 4 m, reaching a maximum depth of about 40 m (at the centre). Another W-E survey was acquired using an electrode spacing of 2 m and a roll-along technique to reach 254 m in length and a maximum depth of about 20 m (Fig. 8A; ESD Fig. 2A).

GPR is a geophysical method that emits pulses of high-frequency radio waves to image the subsurface. In the Gelat plain (Figs. 8, 9; ESD Fig. 2A, B), centre frequencies of 400, 100 and 30 MHz were used to investigate increasing depth range (about 4.5, 10 and 25 m, respectively), at the expense of lower vertical resolution (about 0.12, 0.5 and 2 m, respectively). GPR survey lines were acquired using a GSSI SIR-3000 radar with 100 and 400 MHz shielded antennas recording 20 traces per meter in order to investigate the geometry and continuity of the fan and valley deposits, and to locate the water table. The W-E survey lines at 400 MHz include profiles along the Trenches T2, T4 and T5, T3 and T1 (ESD Fig. 2A, B). Four survey lines at 100 MHz were acquired in the W-E and N-S directions. Several GPR W-E and N-S survey lines across the plain and the lake outlet were also completed later at 30 MHz in order to characterize the bedrock depth and geometry and the water table.

3. Morphometry, landforms mapping and geophysical results

3.1. Morphometry of maar lakes and Lake Pavin

Being c. 6700 years old and having a mid-latitude temperate climate, Pavin exhibits the high aspect ratio, depth ratio, and rim height/diameter ratio typical of youthful maars (Table 1). Table 1 displays morphometric characteristics of Pavin compared to those of similar, recent meromictic maar lakes, and following the global database by Graettinger (2018). The prominent Pavin maar shows high-angle rim slopes despite its middle Holocene age. The contrast between the inner crater rim slopes (>33°), cut through predominantly pre-eruption diverse deposits and the outer crater rim slopes (10–25°) made up of maar tuff, is similar to slope contrast observed in youthful maars. The rim is generally high due to the 40 m lava cliffs reamed out by the crater, crowned by thick (6–15 m) tuff, and to the total crater depth (from the rim top) exceeding 132 m on average (Table 1).

The prominent maar results from a combination of three factors (Figs. 1, 2): (1) The dispersal of erupted pyroclastic deposits (a volume of 5.2×10^7 million m^3 over 146 km^2 according to Leyrit et al., 2016), has contributed to decrease the contrast between the rim and the surrounding, subdued landscape. The ratio of proximal tephra (including ballistic

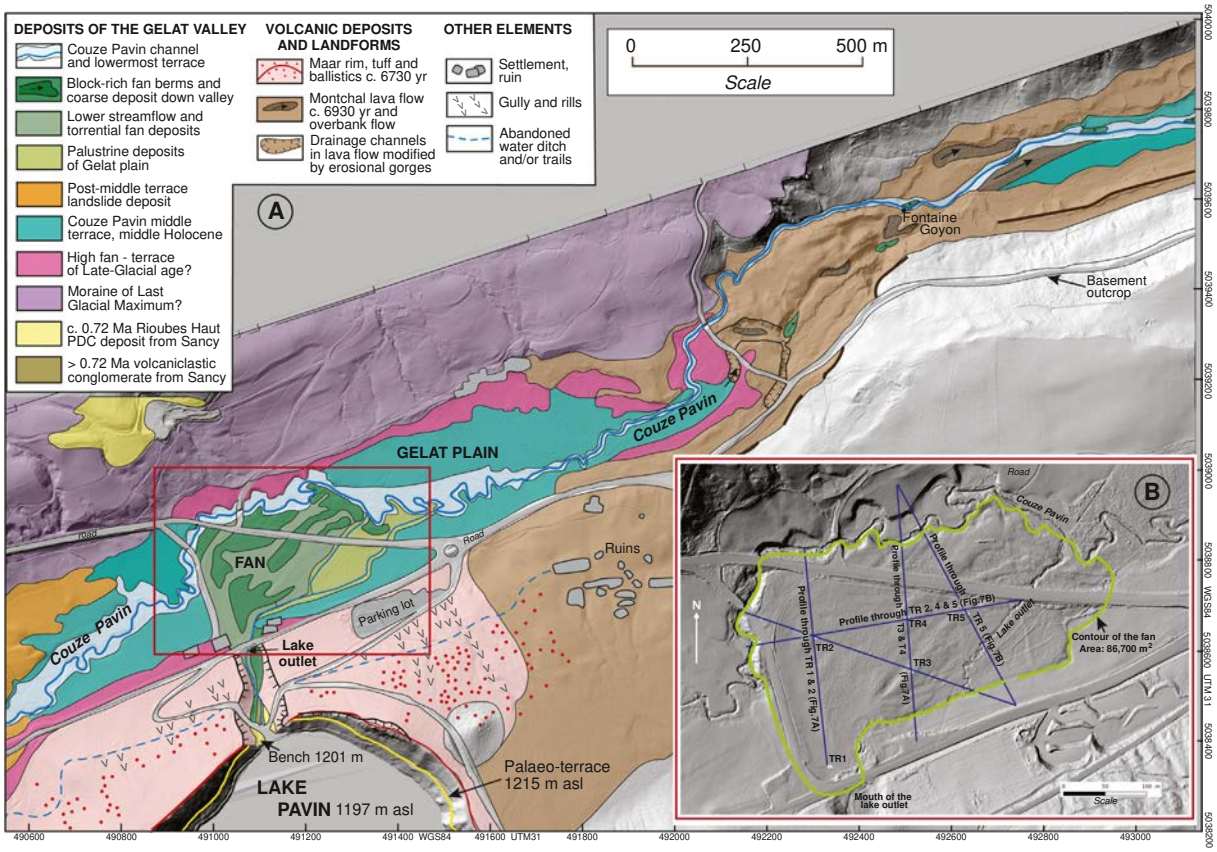

Fig. 3. A. Geological and geomorphological map of the alluvial terraces and fan in the Gelat (Couze Pavin) valley. Inset **B**. LiDAR-derived DSM of the Couze Pavin valley and Gelat plain showing the extent of the fan, the location of the stratigraphic trenches and auger drilled sites along cross section profiles, and the sampling sites of ^{14}C analyzed material. Perpendicular and transverse lines indicate topographic profiles going through trenches and drawn in Fig. 7A and B.

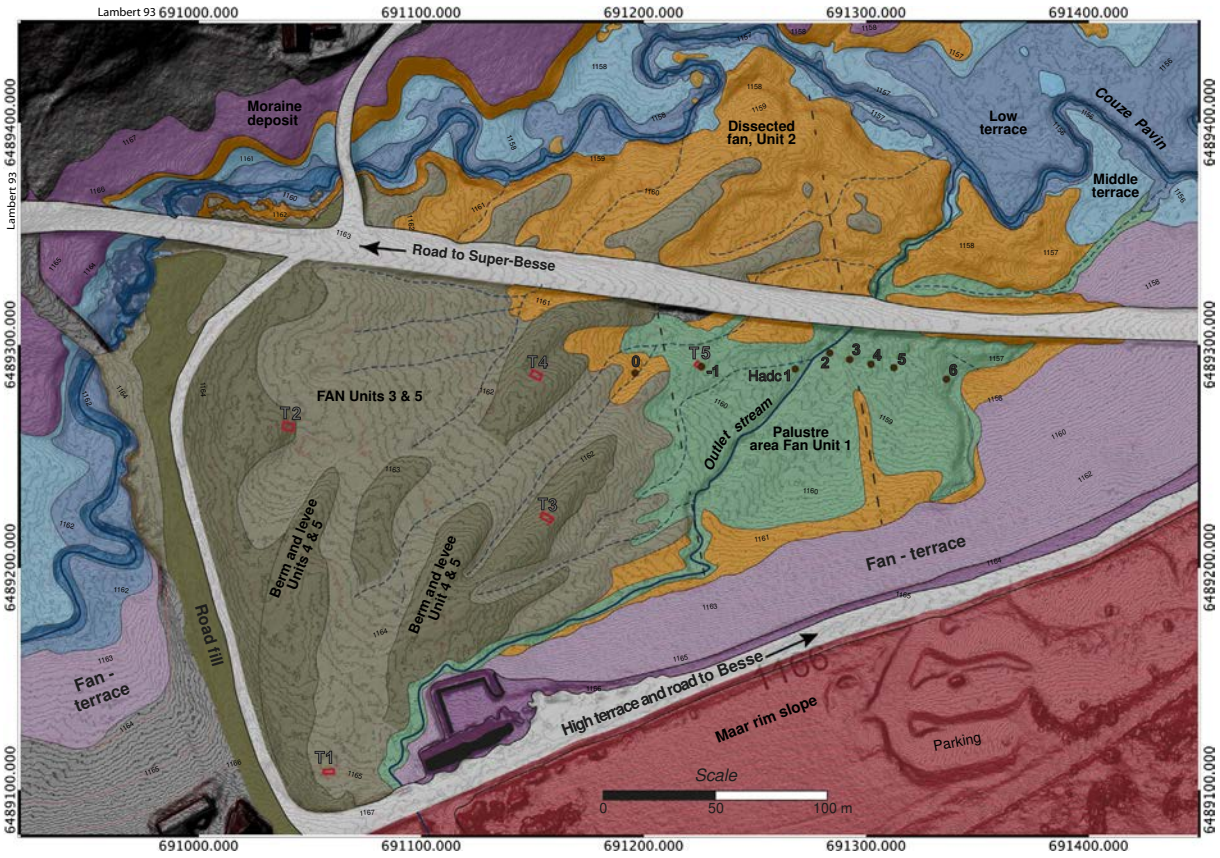

Fig. 4. Geomorphological and geological map of the fan draped on the 1 m resolution drone-derived DSM (2015; photogrammetric survey carried out by Technivue Co.; x and y accuracy within 1 m, z ± 0.12 m; resolution 0.25 m/pixel). Hadc along with numbers 1–6 refer to hand-auger drilled cores of Fig. 7B.

blocks as far as 1.5 km from the lake centre) over the total volume of erupted deposits is 0.43–0.59. If the fine distal ash 'lost' during the maar eruption is added to the total volume, the ratio decreases to 0.40, which does contribute to abate the abovementioned contrast; (2) The low-relief surrounding topography (except for the Montchal cone cut by the south maar rim, Figs. 1, 2) consists of subdued, Quaternary lava flows mantled by glacial deposits. Pre-existing glacial valleys were smoothed out by valley-confined pyroclastic-flow deposits from Pavin and the Montchal lava flows (Figs. 1 to 4); (3) The erosion processes may not have acted severely on the rim outer slopes shortly after the maar formation, as no gullies were observed at the base of the tuff deposit. The relatively coarse size and porosity of the tuff likely prevented the pumice-rich deposit from incision shortly after the eruption.

Pavin maar belongs to the first geomorphic category 'I' described by Seib et al. (2013) as 'easily recognizable by the presence of a ring-shaped tuff rim and steep slopes, and flat crater floors separated by well-marked knick lines from the inner slopes'. Pavin maar also corresponds to lake stage 'B' of Büchel (1993), following the initial stage A, and the 'initial stage 1' (i.e., positive landforms, several hundred meters wide, with lake sediments) of Németh (2001).

3.2. Exceptional features of Lake Pavin maar

1. The high-relief Pavin maar is paradoxical. The position above the surrounding subdued Monts-Dore volcanic and glacial landforms (Fig. 1B, C; Glangeaud, 1916) should not have shielded the maar from erosion, but the strong depth ratio (0.07; Table 1) and abundant lava cliffs sustaining 41% of the rims favour the mechanical resistance of the maar. Lava cliffs stem from the Montchal cone to the SW and NW, while older lava flows from Sancy volcano were cut by the NW rim (Fig. 1). The impounded lake is perched 40 m for the current lake at 1196.32 m (based on DSM data, henceforth 1197 m) with limited (±30 cm) seasonal fluctuations (Jézéquel et al., 2011), above, and adjacent to, the 350 m-wide and 70 m-deep glacially-shaped Couze Pavin bottom c. 1056.50 m asl at the confluence of the outlet with the river (Figs. 1B, 4). The perched location has favoured incision and headward erosion of the lake outlet with a high slope gradient (0.177) towards the Couze Pavin valley located at a short distance of 220 m. On the south side of the dam, the upper part of the lake is impounded behind the natural dam c. 23 m high at the knick point, but the crater lake bottom to the south is 35 m deeper than the Couze Pavin valley bottom to the north (Figs. 1B, 3). We suggest the perched maar index (PMI; Table 1) to assess how a maar lake dam is liable to be eroded, either by outflow incising the rim saddle or by headward erosion of the outlet: PMI is 0.57 from the dam height 23 m and the elevation difference 40 m between the lake and the river channel bottom 510 m away. For the purpose of comparison, Lake Nyos PMI is 0.20, the nearest drainage baseline is 2.3 km away, and the impounded lake volume is 7.5 times that of Lake Pavin (Table 1).
2. The lake is impounded behind a 42 m-long × 40 m-wide × 23 m-high dam made up of three formations (Fig. 1B, 3, 5), in stratigraphic order: (1) A 70 m-thick block-and-ash flow (BAF) deposit that crops out down at the gorge knick-point (Figs. 1B and 5). (2) A c. 20 m-thick, indurated, volcaniclastic conglomerate deposit from Sancy volcano, the youngest edifice of the Monts-Dore massif (Baubron and Cantagrel, 1980) rests on, and seems inset in, the BAF deposit (Fig. 5). The present lake level at c. 1197 m lies near the top of the volcaniclastic, closed framework indurated conglomerate deposit with compositionally mixed, subangular pebbles and cobbles. First mentioned by the engineer Gautié (1867), the conglomerate

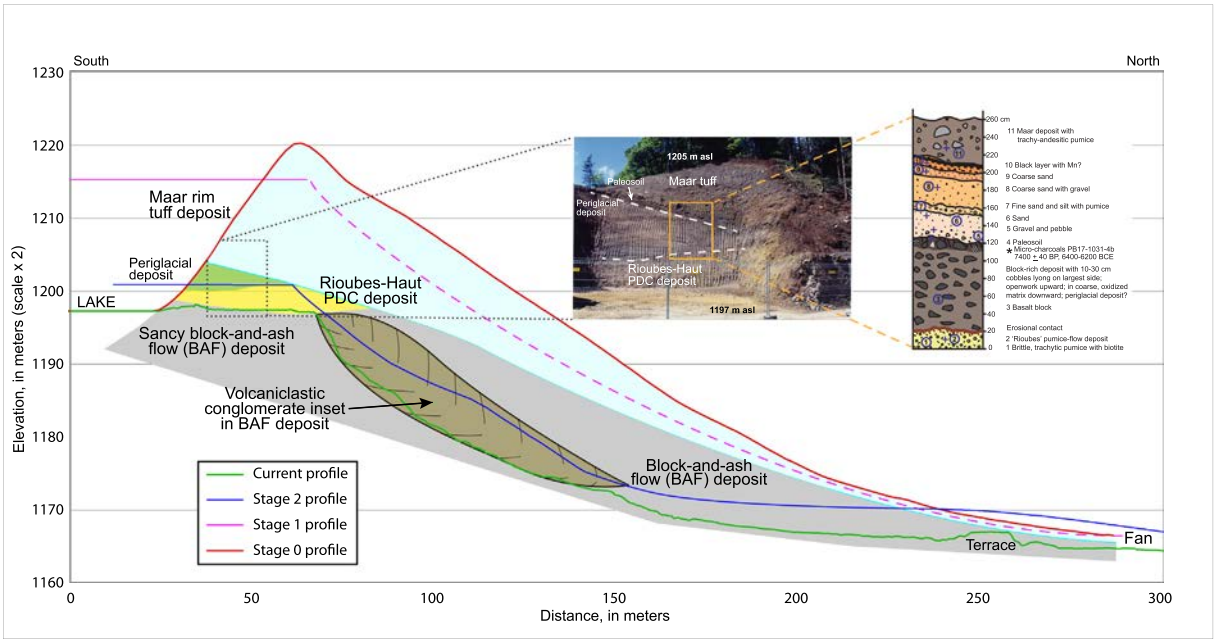

Fig. 5. Longitudinal profiles of the outlet gorge from south (lake shore) to north (Gelat fan) showing how the four channel profiles were assigned to stage 0 (maar initial rim, orange line), stage 1 (1215 m terrace, purple dashed line), stage 2 (1201 m bench, dark blue line), and stage 3 (current outlet channel, green line). The 8 m-high stratigraphic section on the east slope of the lake entrance is shown (linked to the rectangle on the left handside), as well the 2.60 m thick section depicting part of the maar rim deposits and underlying deposits. Both sections have been inverted (from left to right) in order to match the longitudinal profiles of the outlet gorge (from south to north). Note of caution: thickness of the deposits varies locally (e.g., Rioubes- Haut tuff, 4.5 m thick on the east side, up to 8 m on the west side of the dam). The profiles were drawn along the west slope of the lake dam and the outlet gorge.

forms the resistant headwall of the gorge at the top of the dam, although weathering and fracturing are pervasive. (Figs. 5 and 6A, B, C). (3) The 4.5 to 8 m-thick Rioubes-Haut pyroclastic density current (RH PDC) deposits rests unconformably on the first and second formations. The RH PDC deposit that crops out locally on the south and north edges of the maar (Figs. 1, 3), has been re-dated at 0.718–0.723 Ma (Nomade et al., 2014) near the eponymous farm about 0.75 km north of the maar and at the same elevation.

3. The local stratigraphy and structural contacts have guided the incision through the north rim saddle down to the incised notch (Figs. 1B, 5, 6). The north rim saddle is about 550 m long, 60–120 m wide, and 25 m lower than the average rim top surrounding the maar. In the middle of the saddle, a younger, 20 m-deep and 40 m-wide, incised notch has guided the lake outlet (Figs. 1, 2, 3). The saddle is a broad and shallow depression in the loose maar tuff and RH PDC deposit, whereas the V-shaped notch has been cut through the PDC deposit down to the top of the massive conglomerate. The anomalous contact between the PDC deposit and the conglomerate at the gorge headwall is due to fracturing and/or landsliding (Fig. 6C). The notch location coincides with N10°*E*-trending faults detected in the maar area and the PDC deposits on the east slope of the lake dam, which offset the older WSW-ENE and WNW-ESE faults (Fig. 1A; De Goer de Herve, 2000).
4. The outlet, also fed by lake leakages through the north dam, has formed a gorge that links the lake at c. 1197 m with the Gelat plain to the north at 1160 m (Couze Pavin channel). The short (210 m to the fan apex) and narrow (70 to 100 m) gorge is steep-sided with a slope of 18.30% (Figs. 3, 5). Such an outlet gorge is too big with respect to the current outlet and average discharge (50 l/s), while its channel, crowned by the 10 m-high, 70 m-wide, and 90–100 m-long headwall in the indurated conglomerate, displays a steeper shape than the profiles of other Couze Pavin tributaries.

3.3. Lake Pavin shoreline and preserved lake benches

The current lake shoreline can be divided in two parts: the erosional part consists of lava cliffs; the depositional part consists of screes (Fig. 9.3 *in* Thouret et al., 2016). The erosional shore, on the east and south edges of the lake, is characterized by a narrow shoreline above deep water without a lake terrace. A narrow <3 m terrace, termed a *beine* by lake geomorphologists (e.g., Provencher and Dubois, 2008) has been formed by scree or rock fall from adjacent cliffs (Fig. 9.3 *in* Thouret et al., 2016). On the western lake edge, the beine is slightly larger due to runoff and debris redistribution from screes or rock falls, and small deltas formed in the NW and SW corners of the lake. The erosional and depositional pattern of the lake shore is also a result of wave action, which is more important on the eastern edge than the western side, but wind action on waves is limited by the high maar rims.

A lake beine is both an erosional (bench) and constructional (terrace) landform. The cut-and-fill beine consists of an erosional bank cut in the slope (Fig. 2C) with a gentle slope < 5–15° (in contrast to the average 33° rim slope angle) and a constructional bench made up of coarse material together with plant debris. The submerged (<1 m deep) constructional beine is composed of coarse material (blocks, cobbles and pebbles) that lay flat mimicking a pavement, often mixed with gravel and plant debris, 2 to 4 m wide above a steep talus slope connected to the deep lake. The paved beine near the north, NE and NW shoreline, which was walked on by Legrand d'Aussy (1794–1795) in 1787–1788, has been barely submerged by the mid-19th century works for fish introduction. The level of the lake was artificially stabilized when the outlet was channeled in 1859–1860, and occasionally earlier with clods of earth (Lecoq, 1835) (Fig. 1D).

The LiDAR DSM has enabled us to detect one key landform on the inner maar slopes; a terrace at 1215 m asl, i.e., +18 m in elevation above the current lake level (Figs. 2, 6D). The colour-coded slopes indicate a discontinuous, narrow (<3 m) bench cut at 1215 m asl around the rim (Fig. 2B, C). Three characteristics mark this terrace attributed to the Stage 1 highstand: the gentle slope (5–15°) of the bench contrasts with the otherwise steep slope (25–35°) of the rim (Fig. 2C), the bench has been cut in the underlying deposit, and it is also made up of sand, gravel and pebbles, now covered by a soil and colluvium. This deposit may be the beine of the highstand lake, now eroded. Charcoal found at the contact between the colluvium/soil and the sand and gravel deposit cut by

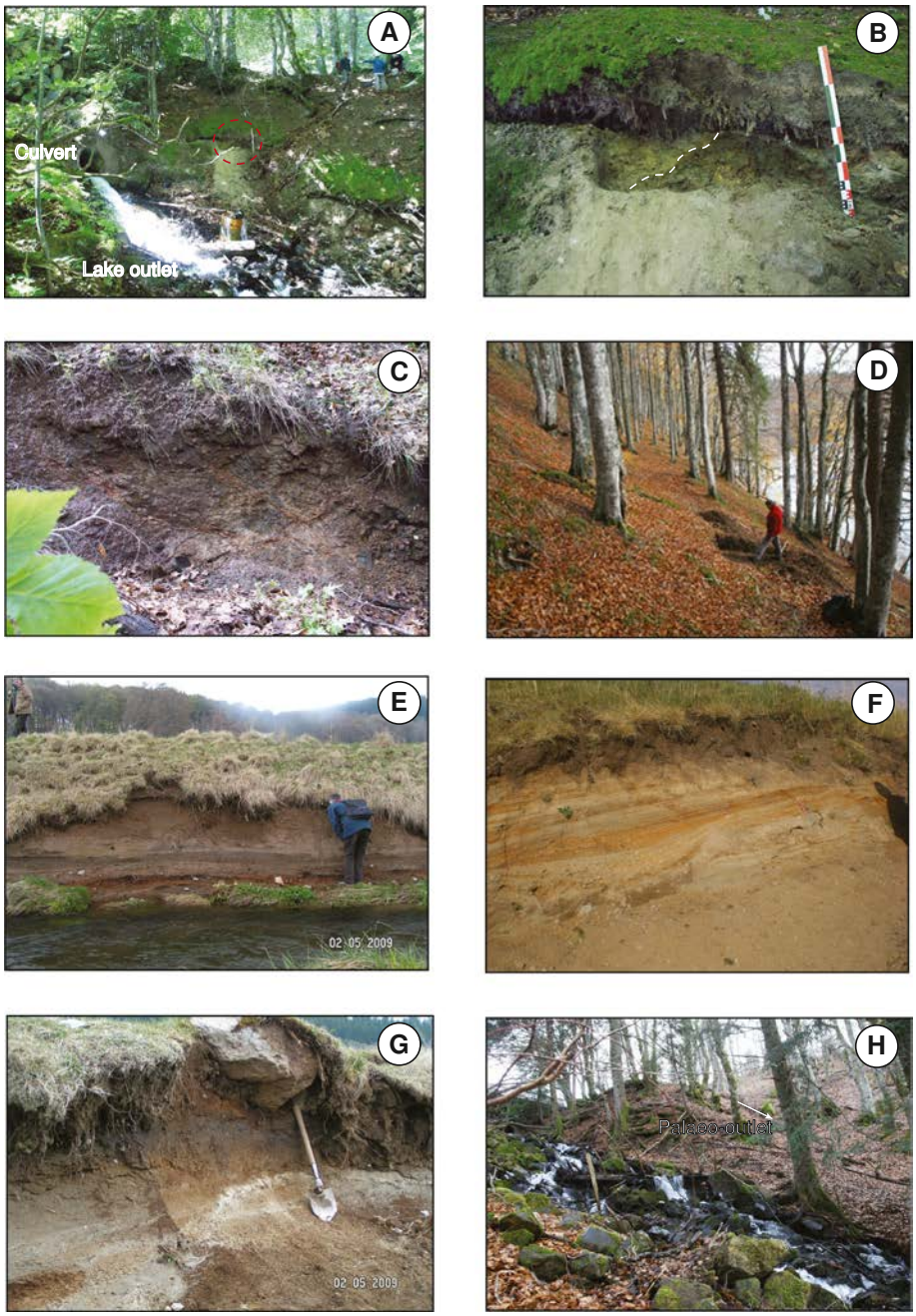

Fig. 6. Pictures of stratigraphic sections, sample sites and deposits, and landforms attributed to successive lakes. **A**. Outlet west bank of the lake outlet, showing the contact between the Rioubes- Haut PDC deposit and the conglomerate. Circle indicates location of the picture B. **B**. Contact (dashed white line) of the RH PDC (to the left) resting unconformably on the conglomerate. **C**. Weathered and fractured, but indurated volcaniclastic conglomerate. **D**. Bench at 1215 m asl under forest on the inner rim slope attributed to the Stage 1 lake shoreline. **E**. Middle terrace along the Couze Pavin south bank showing the maar deposits at the base. **F**. Couze Pavin River south bank section showing reworked maar deposit in the middle terrace of Middle Holocene age. **G**. Organic clay layer dated at 2530 ± 30 BP, i.e., 540–570 BCE that rests on top of reworked maar deposit and is overlain by the fan material. **H**. Abandoned outlet channel under the forest canopy in the west side of the outlet gorge headwall (to the right side of the active emissary). This outlet channel was linked to the bench and weir c. 1201 m during the short interval between Stages 2 and 3.

the bench yielded relatively recent ages between the 14th and 16th century (Table 2; Fig. 2C). We interpret this result in two ways: the charcoal stems from forest fires or fireplaces around the lake that have induced slope colluvium activity, and/or they indicate that the lake level was preserved over a long period until the late Middle Ages.

Another bench about 9 m wide, with a gentle slope towards the outlet gorge, is preserved at 1200.65 m asl (henceforth c. 1201 m) on the west side of the dam, c. 4.35 m above the current lake (Figs. 1D, 2B). The engineer Gautié (1867) from the French Bridges and Roads Dept. carefully measured the dam landforms in 1867, drawing a bench about 15 m wide at the top and 28 m wide at the base, with a top surface at 1202 m asl, c. 5 m high (at the knickpoint with the west slope of the notch) above the outlet at that time. Part of the bench has been removed when the notch bottom was reshaped, and platform, road, and embankment built up after 1950. We interpret the preserved bench as a witness to the lake Stage 2 shore at c. 1201 m, i.e., about 14 m below the lake terrace Stage 1 at 1215 m. A similar bench, albeit discontinuous, can be recognized elsewhere around the lake: small fans located inside the amphitheater open on the north flank of the Montchal cone shows a front cut at about 1201 m in elevation on the SSW rim (Fig. 2B). The

W and SW segments of the round-the-lake trail, set up between 1199 and 1201 m in elevation by the Forest service around 1850, likely re-used the lake shoreline (Fig. 2B).

3.4. Geological and geomorphological mapping of the Gelat valley and fan

Relationships between the high, middle, and low terraces along the Couze Pavin and the growth of the Gelat fan are as follows (Figs. 3, 4): (1) The fan pushed the Couze Pavin 250 m towards the north bank of the valley; (2) The fan deposits overlay the middle alluvial terrace of Couze Pavin, the base of which includes the 6700 yr-old maar deposits (Fig. 6E, F; Thouret et al., 2016); (3) The 1.5 m-high, lowermost terrace of Couze Pavin is inset 2 to 3 m in the fan deposits, so is younger (Figs. 3, 4); (4) The high terrace, probably of Late-Glacial age, is preserved on the north side and upstream of the Couze Pavin valley. This high terrace precedes the maar formation as the tuff mantles the high terrace. A gentle slope termed 'fan terrace' links the maar rim outer slope with the residual high terrace on the south side of the valley (Figs. 3, 4).

Despite the inconspicuous, gentle slope landform, the fan formed by the lake outlet across the Gelat plain was recognized from aerial photographs taken in 1955, preceding farming impacts (Fig. 1E; Lavina and Del Rosso D'Hers, 2009). The principal fan feature comprises four finger-shaped berms or levees separated by shallow and narrow rill channels (Fig. 4). The Couze Pavin meanders near the north edge of the Gelat plain and along the gentle slope (1.27%) of the alluvial valley. The flattish valley is due to the voluminous Montchal lava flow that dammed the Gelat plain down valley near a glacial-shaped rock bar to the East (Figs. 1, 3). The 200 m-wide Gelat plain contrasts with the steep (6%) and narrow (100 m) Couze Pavin valley downstream of the lava dam. As a result, the post-glacial Gelat plain acted as a basin hosting palustrine deposits that preceded the fan formation. Although Glangeaud (1916) postulated "a lake 2 km long and 20 to 40 m deep" and his cross section depicted lake sediment in the Gelat plain (*in* Sime-Ngando et al., 2016, p. 107), no lacustrine deposit crops out along the Couze Pavin where the river cuts the dam down by 3 to 5 m into the lava flow. From the ^{14}C-dated top of the palustrine Unit 1 (Fig. 6B) and river banks (Fig. 6G) in the Gelat plain, the palustrine basin existed between the 8-6th century BCE and the 5th century CE (Table 2). The basin drained probably at the time Lake Pavin started to fall from its highstand Stage 1 level.

3.5. Geometry and stratigraphy of the valley deposits based on geophysical results

Electrical Resistivity Tomography (ERT) and Ground-Penetrating Radar (GPR) survey sections across the fan, the Gelat valley and the outlet gorge (ESD Fig. 2A) provided data to depth > 20 m. Different penetration depths and resolutions allow us to constrain the spatial distribution of several formations, although they do not provide direct information on the composition of sub-surface units (Figs. 8, 9; ESD Fig. 2B).

1. The shallowest formation, from the surface down to 2.5 or 3.5 m deep (3 m on average), is relatively resistive (1000–2500 Ω·m), as observed in the W-E trending ERT profile (Fig. 8A). This unit likely corresponds to the streamflow fan deposits, 2 m thick on average and up to 3.20 m thick as measured in trenches (Fig. 7A, B) and analyzed from high frequency radar profiles. Local decreases in resistivity (800–1200 Ω) at about 72 m, 130 and 191 m in Fig. 8A are likely

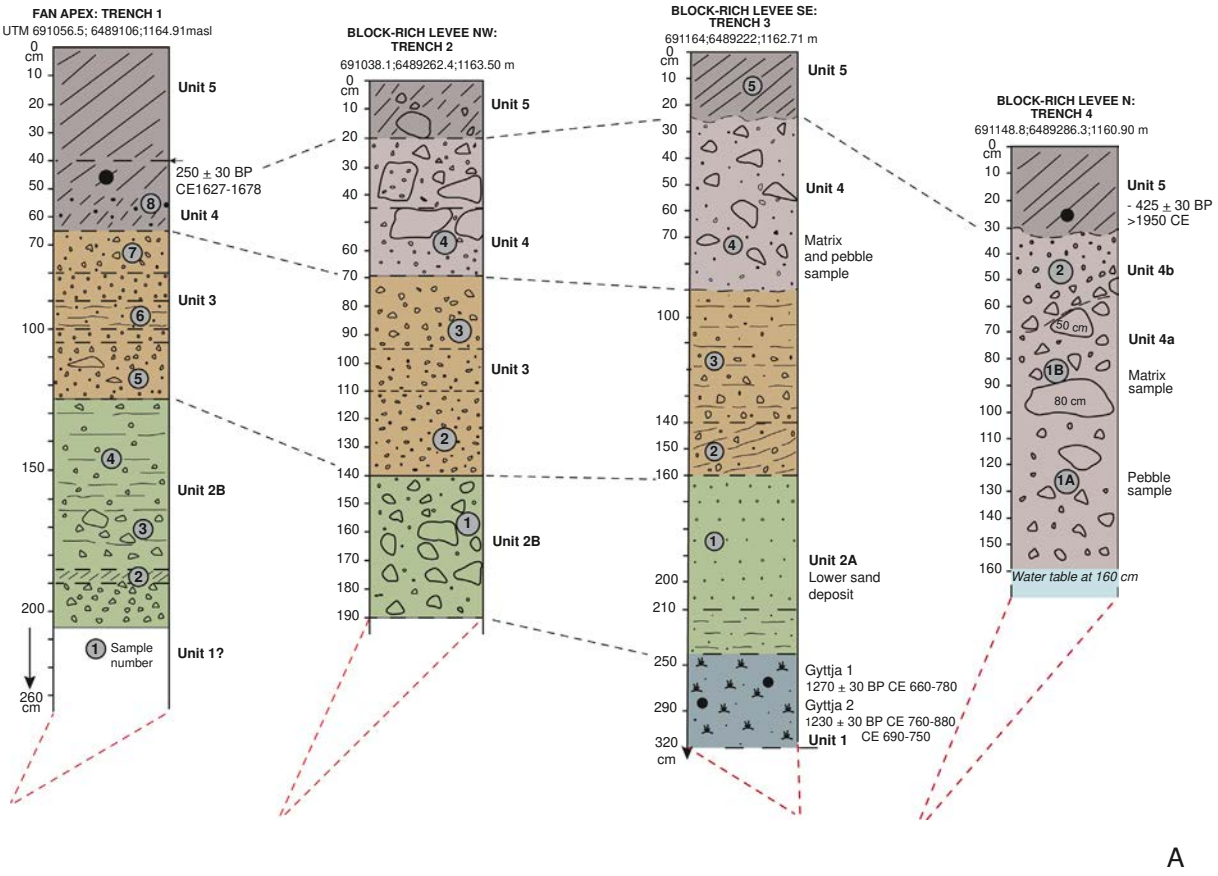

Fig. 7. Stratigraphic sections from trenches dug in the fan and auger drilling sites in the east sector of the fan located along south-northward and west-eastward profiles. **A.** Perpendicular profile of Fig. 3B showing the location and stratigraphy of trenches 1 and 2; Perpendicular profile of Fig. 3B showing the location and stratigraphy of trenches 3 and 4. **B.** Transverse profile of Fig. 3B showing the location and stratigraphy of Trenches 2, 4, and auger drilled cores; perpendicular profile of Fig. 3B showing the location and stratigraphy of Trench 5.

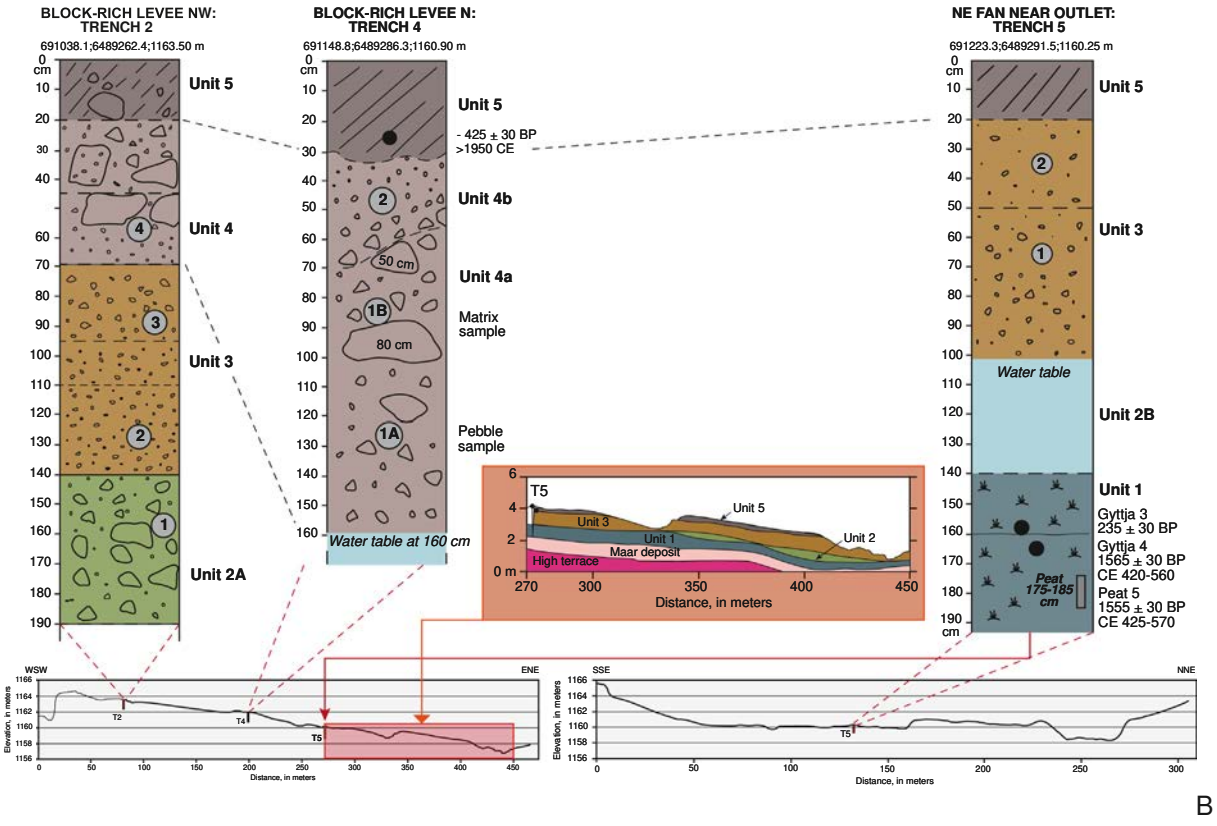

Fig. 7 (*continued*).

associated with rill channels between the topographic levees of the finger-like berms across the fan (Fig. 4). The lower surface resistivities of this surficial layer to the east (beyond 192 m distance) and the small discontinuity at about 230 m distance coincide with the lake outlet stream and the shallow water table.

2. The formations between 3.5 m and about 12 m in depth show a high conductivity (resistivities < 1000 Ω·m) in both ERT sections (Figs. 8A, 9A), suggesting high-water content. The upper boundary is subhorizontal and marked by a sharp vertical resistivity gradient gently approaching the surface towards the palustrine deposits that crop out near the outlet stream in the eastern fan area (Figs. 4, 8A). Consistently, the 100 MHz signal undergoes significant attenuation below a well-marked subhorizontal reflector (Figs. 8C, 9B). This radar interface (equivalent to the >900 Ω·m resistivity contour) diminishes from 3.5 m deep to the W to less than 1 m deep downslope near the stream to the E, which matches with the water table top observed in trenches T1 (2.2 m), T2 (2 m), T3 (1.6 m) and T5 (1 m) (Fig. 9B; ESD Fig. 2B.c). Another conspicuous dielectric interface at 100 MHz is found from 3 to 4 m on the valley sides to 8 m deep in the valley centre (N-S section, ESD Fig. 2B.b) and westward (Fig. 8C), sometimes imaged at 30 MHz (line 345, Fig. 9C, D). This interface corresponds to the minimum resistivities as low as 300 Ω·m in the centre of the conductive ERT unit (Figs. 8A, 9A). The W-E trending ERT and 100 MHz GPR cross sections show that the intermediate, water-rich formation thickens and deepens eastward in the marsh area of the fan near the Couze Pavin channel. We interpret the conductive layer attenuating the radar signal from about 3 to 8 m in depth as water-rich palustrine deposits 1–3 m thick that rest on the 1–2 m thick maar deposit (see Fig. 7B), the thickness of which is variable, as shown by other radar interfaces at 100 MHz (Fig. 9B; ESD Fig. 2B.b).
Deposits below the maximum conductivity values show a vertical resistivity gradient from c. 8 m depth down to the basement at 12–15 m (maximum resistivities, Fig. 8A), more heterogeneity in 100 MHz GPR signals (Figs. 8C, 9B; ESD Fig. 2B.b), and a lack of continuous deeper reflectors at 30 MHz (Fig. 9C; ESD Fig. 2B.a). This gradient likely reflects a transition to less dense but coarse deposits such as moraine or thick fluvio-glacial sediments for the Couze Pavin catchment (Fig. 4), and/or the weathered and fractured top of the basement.
3. A deep, very resistive layer (>3000 Ω·m, Fig. 8A) at least 20 m thick is found in both W-E and N-S ERT pseudo-sections throughout the entire valley (Figs. 8A, 9A). Its horizontal, tabular upper limit lies between 12 and 15 m in depth below the fan surface at 1162 m (Fig. 8A), and can be traced, though discontinuously, along a few GPR profiles at 30 MHz (Fig. 9C, D; ESD Fig. 2B.a; line 352, ESD Fig. 2B.a) and below which the radar signal abates. This suggests the presence of basement at c. 1150 m asl near the valley floor. Gneiss/migmatite outcrops at c. 1150 m asl were mentioned by Vimont (1889), mapped by Glangeaud and Boule (1925), and are visible about 1 km ENE from the Gelat plain along the road crossing the north-facing Couze Pavin valley wall (Fig. 3). The depth to basement likely increases from about 12 m in the valley (e.g., line 352 at 30 MHz, ESD Fig. 2B.a), in agreement with ERT data, to nearly 20 m below the sloping surface in the outlet gorge in GPR sections, uncorrected from topography (line 345, Fig. 9C, D; line 352, ESD Fig. 2B.a). Taking into account the rising slope along the outlet towards the lake dam, the net elevation of the basement likely gently rises towards the crater. Above this interface, the outlet gorge infilling shows several layers despite the poor resolution (about 2 m) at this radar wavelength (ESD Fig. 2B.a).

4. Stratigraphy and sedimentology of the fan deposits

4.1. Stratigraphy and ^{14}C chronology of the plain and fan deposits

Five deposit units have been identified in the Gelat plain and fan, based on the stratigraphy observed in trenches, along the river south

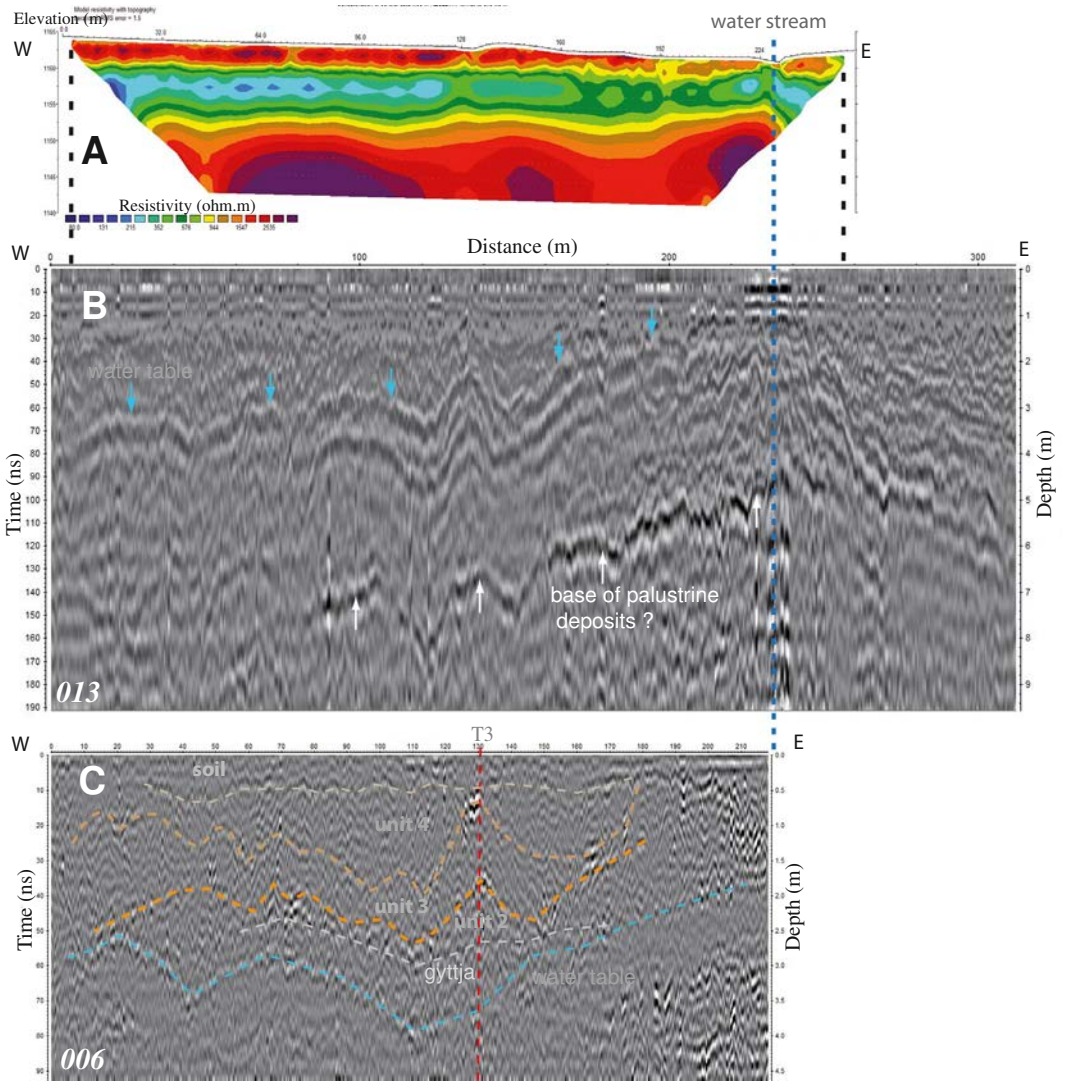

Fig. 8. A. Resistivity model including topography from WNW-ESE ERT roll-along LR00060–62, with 2 m inter-electrode spacing. **B**. 100 MHz GPR radargram 013 (not corrected from topography) parallel to ERT line shown in A. **C**. 400 MHz GPR line 006 close to T3, showing fan units.

bank (Figs. 4, 6A, B, G, 7), and on geophysical surveys (Figs. 8, 9; ESD Fig. 2A, B). Table 2 displays the chronological dataset based on thirteen ^{14}C dated deposits. ESD Fig. 3 shows the 2D sections of the trench walls, including the layer grain size and interpreted Units. Figs. 10A–D; ESD Tables 1, 2 display the lithological components from fine (1 mm) and coarse (8, 16, 22.4 and 50 mm) fractions of each of the layers. Typical features of the fan stratigraphy, such as irregular and imbricated layers and cut-and-fill channels, are imaged in several GPR profiles at 400 MHz (Fig. 8C; ESD Fig. 2B.b.d).

1. Unit 1 includes palustrine deposits 1–2 m thick that consist of gyttja and plant debris with a few peat layers. The lowermost peat layer overlying the maar deposit along the Couze Pavin south bank, underlying the fan units, was dated (SacA46776, Table 2) between the mid 6th century BCE and late 8th century BCE. The peat layer overlies reworked maar deposits that form the base of the middle terrace (Figs. 4, 5, 6B, E–G). The terrace contains the maar tuff deposit that has been reworked between 6700 and 2700 years ago and mixed with alluvium. Downcutting of the Gelat plain since the 6-8th century BCE has been induced by the Couze Pavin erosion (Fig. 4), its channel having incised >3 m in the lava-flow dam downstream.
   The upper part of Unit 1 at least 1 m thick crops out in the eastern area of the fan where erosion has uncovered the most recent fan deposits. The W-E ERT section (Fig. 8A) shows that the palustrine deposits of Unit 1 can be traced towards the east end near the tributary of the Couze Pavin across the east fan area. This fan area has been eroded while the lake outlet shifted from the mouth of the gorge towards the east (Figs. 3, 4B), meanwhile the Couze Pavin has incised the Gelat Plain since the fan growth. Gyttja has been dated in several sites from the lowermost stream bank across the fan, in trenches 4 and 5 located east of the fan, and from hand auger drilled cores (Figs. 4, 7B). Three ^{14}C ages indicate that the top 40 cm of Unit 1 was deposited between the 5th–6th century CE and the 7th–9th century CE (Trenches 3 and 5, Fig. 7A, B).
2. Unit 2 is made up of 0.65–0.85 m-thick alluvial deposits that consist of beds including sand, gravel and pebbles (Fig. 7A, B). It exhibits two facies: (1) The sand Unit A, 85 cm thick in Trench 3 (ESD Fig. 3), is made up of crudely stratified, fine (56%) and coarse sand (17%) layers. (2) The sand/gravel Unit B is 50 to 65 cm thick in Trenches 1 and 2 (Fig. 7A; ESD Fig. 3), in which lenses of coarse gravel, subrounded pebbles and cobbles up to 20 cm in diameter are intercalated. Unit 2A was deposited by the Couze Pavin across the alluvial plain and Unit 2B by the lake outlet overflow during a high-level lake stage. This period may have included episodes of floods or hyperconcentrated flows, as in Trenches 1 and 2, where Unit 2B is coarser than other layers of the same unit (ESD Fig. 3). Unit 2 is well imaged in radar sections at 400 MHz next to T3 and T1 (lines 006 and 010, Fig. 8C and ESD Fig. 2B.d,

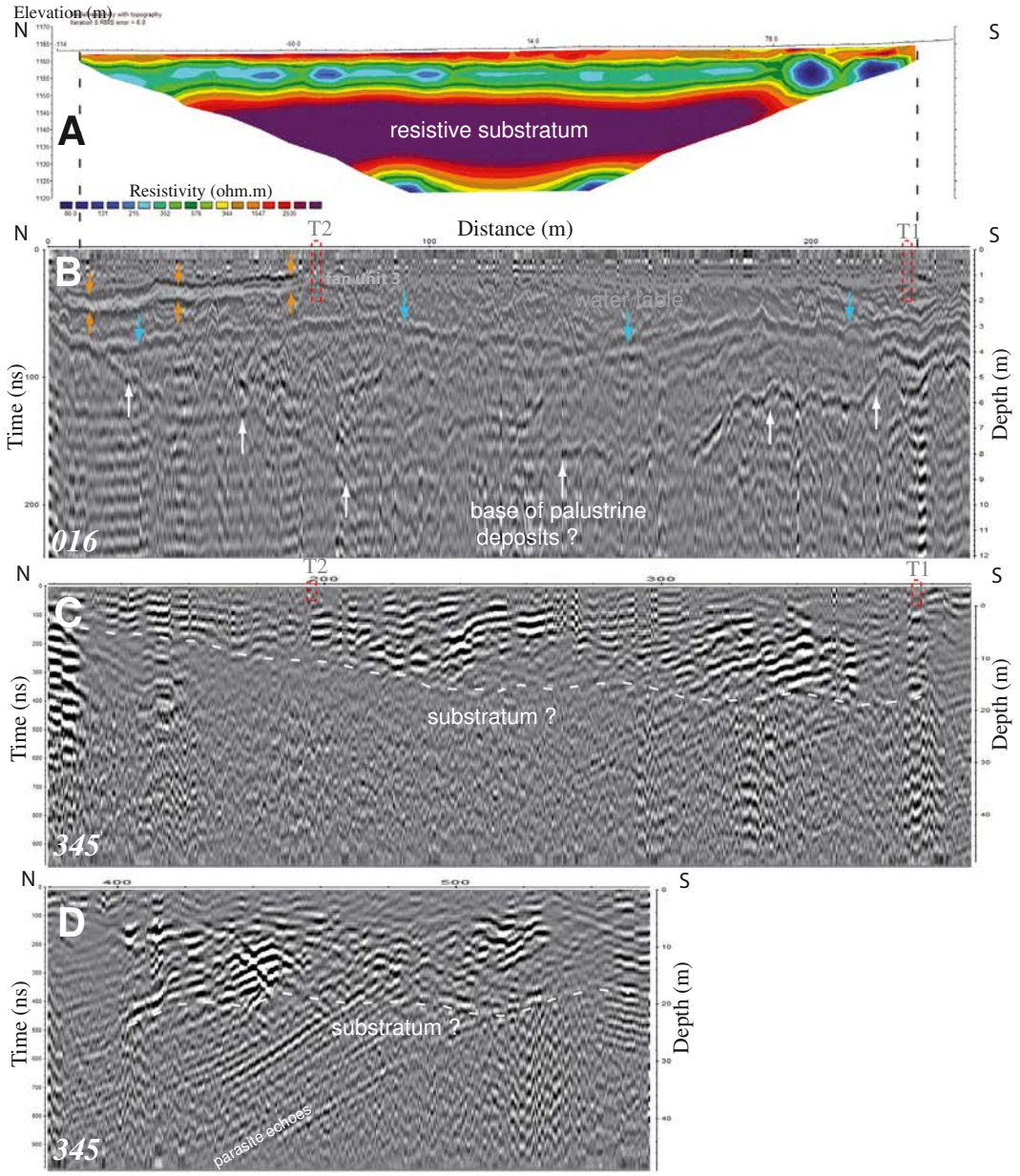

Fig. 9. A Resistivity model including topography, from NNE-SSW ERT acquisition line LR00063, with 4 m inter-electrode spacing. **B**. Ground-Penetrating Radar WNW-ESE line 016 at 100 MHz. **C**. N-S GPR line 345 at 30 MHz across the fan. **D**. The N-S GRP line 345 continued along the outlet gorge. Locations of trenches T2 and T1 are projected onto the profiles.

respectively) showing many long (ten to several tens of m) beds and lenticular layers totaling less than one meter in thickness. Thin, homogeneous layers are more numerous near T3 than T1, in agreement with stratigraphic observations.

3. Unit 3 consists of crudely stratified deposits made up of coarse sand layers alternating with coarse beds including coarse sand, gravels and pebbles (Fig. 6). Unit 3 shows stratified, gravel-rich beds totaling 0.70 m on average with imbricated, subangular pebbles 3–5 cm across (up to 10 cm) and cobbles. A few beds show lenticular lenses and low angle layers with irregular, erosional contacts (Trench 2, ESD Fig. 3). Unit 3 is well imaged by 100 MHz radar signals (lines 013 to 016: Figs. 8B, 9B) over 100 m laterally without substantial changes in thickness. Unit 3 appears rather homogeneous with a thickness of 0.7 m on average (0.5 to 1.3 m). The higher resolution of 400 MHz radargrams allows us to trace in some sections the top and bottom of Unit 3 over 200 m from observed trenches (Fig. 8C, 9B; ESD Fig. 2B.c,d).
4. The massive and coarse Unit 4 ranging from 50 cm to 130 cm thick typically consists of pebbles, cobbles and boulders up to 80 cm in a coarse gravel-rich matrix. Boulders up to 80 cm have been transported up to 250 m from the nearest maar rim slopes. This is the coarsest stratigraphic unit in which angular cobbles and blocks represent 20 to 30% of the deposit. The base of Unit 4 shows a coarse sand sole layer 15 cm thick, supporting inversely graded, angular pebbles and cobbles, sometimes closely packed and resting on their largest side (e.g., Trenches 2 and 4, Fig. 7A; ESD Fig. 3). The 1955 aerial photograph reveals finger-like levees and block-rich berms formed by debris-flow deposits 1 to 2 m higher than the average top of the fan (Fig. 1E). Irregular, cut-and-fill layers, and imbricated deposits across the levees and berms appear clearly in the GPR 400 MHz line 006 (Fig. 8C) in the vicinity of Trench 3 (Fig. 7A; ESD Fig. 3). Unit 4 shows an irregular base about 0.5 to 2 m deep in radar sections (Fig. 8C; ESD Fig. 2B.c), showing a variable thickness between 0 and 1.3 m.

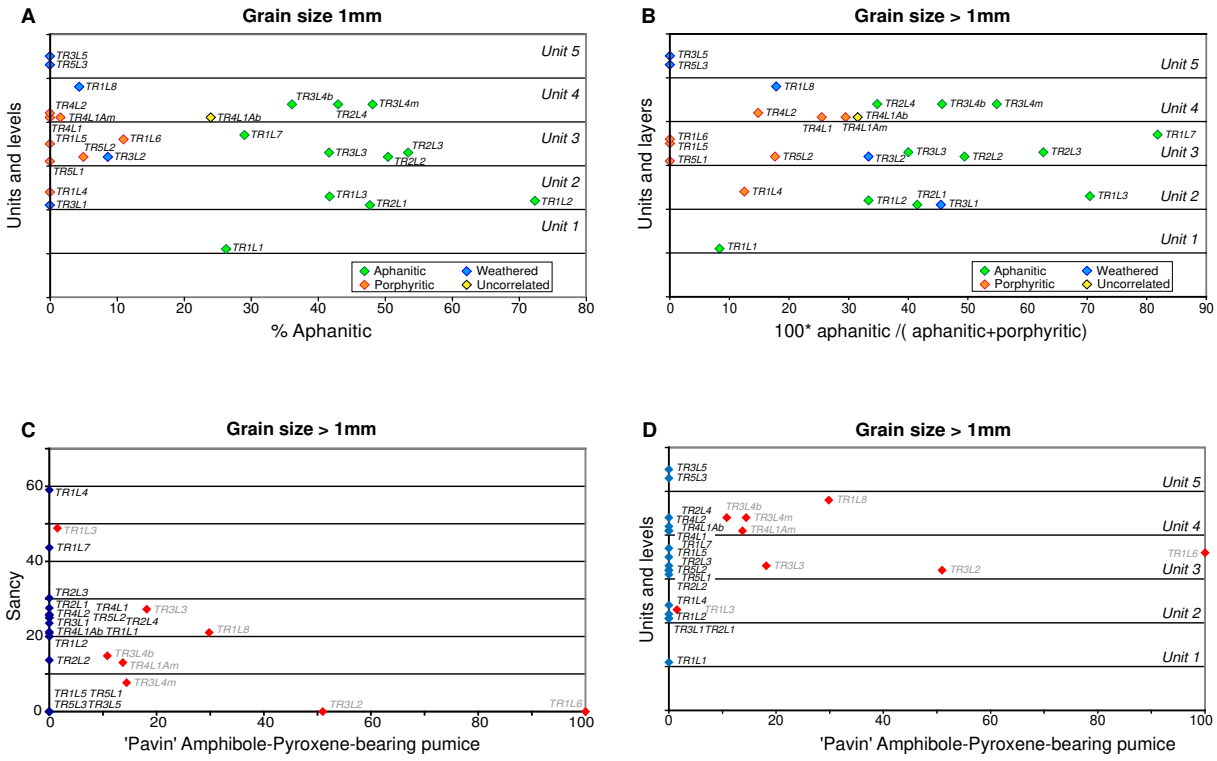

Fig. 10. Lithological componentry of the layers in Trenches 1 to 5 dug in the alluvial fan and Gelat plain (see the Trench stratigraphical Units in Fig. 7A, B and layers in ESD Fig. 3): **A**. Plot showing % Aphanitic clasts per trench and layers in fraction 1 mm. **B**. Plot showing % 100 * aphanitic / (aphanitic + porphyritic) clasts per trench and layers in fraction 8 to 22 mm. **C**. Plot showing 'Sancy' versus 'Pavin' amphibole- and pyroxene- bearing pumice per trench and layers in fraction 8 to 22 mm. **D**. Plot showing % 'Pavin' amphibole- and pyroxene-bearing pumice per trench and layers in fraction 8 to 22 mm.

5. Unit 5 is a 25 to 50 cm thick, fine sand and silt, including some gravels. Repeated plowing techniques have contributed to plane the irregularities of the fan, erode the levees, fill channel rills, and remove the surficial outsized blocks. A thin, reworked soil (20–30 cm) rich in gravel and pebbles overlies the boulder-rich berms (Trench 2), while the 50 cm-thick soil, including gravels, mantle the less coarse deposits (Trench 1, Fig. 7A; ESD Fig. 3). The base of the reworked soil provides a good reflector at 400 MHz between 0.25 and 1 m in depth (Fig. 8C; ESD Fig. 2B.c). The base of the soil Unit 5 in Trenches 1 and 4, dated in order to obtain a minimum age for the berm, has yielded two ages: one is 20th century, the second ranges between 1520 and 1800 CE. This indicates that the underlying Unit 4 has a minimum age prior to the 16th century.

4.2. Correlations and origin of the unit deposits based on lithology

Lithological analysis helps further distinguish the stratigraphic fan Units 2 to 4. We aim to fingerprint the origin of the lithological components of Units 2 to 4 in order to distinguish the maar area contribution from the wider Couze Pavin catchment. Lithological components in the Gelat plain and fan deposits have their source in three catchments: (1) the Couze Pavin valley upstream and west of the Pavin outlet (7.3 km^2, i.e., c. 81% of the total catchments) on the Sancy volcano where erosional processes are active, (2) the Pavin-Montchal catchment of 1.58 km^2 (19%) to the south where erosional processes are weak, and (3) the steep lake outlet gorge 0.02 km^2 (0.2%). The diverse lithologies can be split up in three groups: (1) The Monts-Dore massif contains un-differentiated and aphanitic basalts and basanites; (2) the younger Sancy volcano within the massif includes porphyritic lavas such as trachy-basalt, trachy-andesite, and trachyte in BAF deposit, and RH PDC trachytic pumice with feldspar, plagioclase, and pyroxene. The upper Couze Pavin catchment shares many lithologies with both volcanoes, including the moraine deposits: multiple porphyritic lavas (basalt, trachyandesite and trachyte), and aphanitic basalts. No basement (metamorphic) rocks were found. (3) The Pavin-Montchal group includes lithic clasts with amphibole (amph)- and clinopyroxene (cpx)-bearing pumices in the maar tuff and volcaniclastic rocks from the outlet gorge; scoriae, and cpx- and amph-bearing trachybasalt from the Montchal cone, a minor quantity of basement rocks (gneiss/migmatite); fluvio-glacial deposit with aphanitic lavas.

We divided a total of 4300 grains and clasts in two categories: coarse clasts ranging between 8 and 22.4 mm and fine grains between 1 and 2 mm, because each grain-size fraction contains different lithologies that cannot be correlated based on their sizes only. We retained the following eight components (ESD Tables 1, 2): aphanitic, porphyritic, trachyte, biotite-bearing pumice assigned to Sancy, amphibole-bearing pumice attributed to Pavin, basement, free crystals, and oxidized/weathered grains. Overall, the lithological components help distinguish the alluvial Unit 2, which was principally fed by the Couze Pavin catchment, and the coarse-grained Units 3 and 4 which were sourced from local Pavin-Montchal and Monts-Dore-Sancy lithologies (Fig. 10A–D).

4.2.1. Componentry of 1 mm grains

We used a covariance test for 1 mm-sized grains (n = 2315). Covariance is an indicator of the extent to which two random variables are dependent on each other; higher number thus tends to reflect higher dependency. The first three components, i.e., aphanitic, porphyritic, weathered and undifferentiated (see colored component percentages, ESD Table 1) show a highly significant covariance and they exclude each other, as demonstrated by the three-component graph Lithology 1, ESD Table 1. Two categories (biotite- and feldspar-bearing Sancy pumice) also show high proportions, but their covariance values remain low. Each of the unit/layer couple shows correlations in the covariance ESD Table 1 and Fig. 10A in which they are categorized against the aphanitic component. This dataset is consistent (except for one sample,

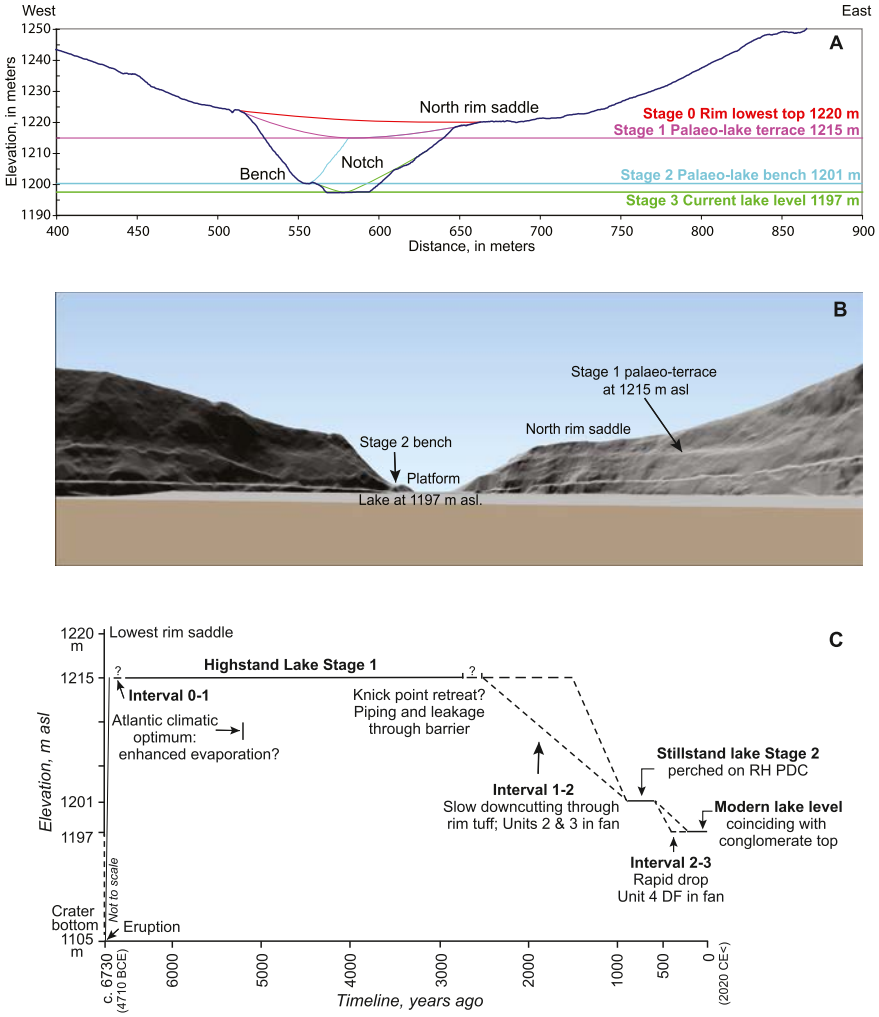

Fig. 11. Summary of Stages 0, 1, 2 and 3 of the evolution of the Pavin maar rim, early lakes and current lake. **A, B**. Topographic profile of the north rim and 2D-view looking north from the lake derived from the LiDAR DSM (Note that x-axis and z-axis scales are different.) The evolution of the northern segment of the Pavin crater rim has been related to the preserved lake landforms, the erosion of the saddle, notch, and the incision of the lake outlet. **C**. Timeline evolution of Lake Pavin showing three Stages (Highstand 1 at 1215 m, stillstand 2 at 1201 m and modern lake level at c. 1197 m asl) and intervals of lake level drops (approximate duration suggested by dashed lines). Processes probably acting during these intervals are indicated.

yellow symbol in Fig. 10A), which allows us to correlate layer and unit couples between the trenches. As a result, porphyritic grains reflect a lithological source in the Pavin maar catchment, whereas aphanitic grains reflect the contribution of the Couze Pavin catchment. Although its number of grains is limited, Layer 1 in Trench 1, attributed to Unit 1, shows a very low proportion of aphanitic grains and zero porphyritic grains. From Unit 2 to 4, each of the layers includes aphanitic grains or porphyritic grains. Unit 5 contains only porphyritic grains. Each layer thus reflects a particular lithological source.

4.2.2. Components of 8–50 mm clasts

EDS Table 2 of the lithological components for the coarse fraction 8, 16.4, 22 and 50 mm (n = 1967) displays the covariance test based on the raw data and % counts. Values of significant covariance are highlighted in orange. The ratio between the numbers of aphanitic clasts and the porphyritic clasts for each of the layers is shown in Fig. 10B. Green labels indicate samples of which the 8–50 mm fraction consists of aphanitic clasts only: a strong correlation exists for the values exceeding 50% of the parameter 100 ∗ Aphanitic / (Aphanitic + Porphyritic) (Fig. 10B). In contrast, the correlation becomes weak below 50%.

ESD Table 2 of covariance shows an inverse relationship between the amphibole and pyroxene-bearing pumice clasts, now termed **'**Pavin', and the aphanitic and porphyritic clasts, as displayed in the graph Lithology 2, ESD Table 2. Red labels in the graph indicate samples that contain 'Pavin' clasts, while the relationship between Pavin clasts and the clasts defined by the ratio 100 ∗ Aphanitic / (Aphanitic + Porphyritic) is inverse. The covariance test in ESD Table 2 also reveals an inverse relationship between the groups of 'Pavin' clasts and 'Sancy' clasts; the latter stands for Sancy trachyte, trachyte with amphibole and Sancy trachyte with biotite. This is shown in Fig. 10C in which red labels indicate samples that contain 'Pavin' clasts.

Overall, the parameter 'Pavin clasts' from the maar lithological source seems robust, despite the limited number of clasts observed in a few categories. Red-labeled samples in Fig. 10D for all 'Pavin' clasts reported in Trenches 1–5 allow Units 3 and 4 to be distinguished, and secondarily, Unit 2 with the sample TR1L3. For example, cobbles and blocks in Unit 4 of the Gelat fan must be sourced at the Pavin maar rim, including the ballistic ejecta observed on the north, NW and NE rims. A small part of the blocks (prismatic, aphanitic lava) may stem from the Sancy lavas ejected as ballistics on the maar rim outer slope, and later removed from the outlet gorge slopes. Today, many blocks sliding on the gorge banks towards the channel point to trimlines from past debris-flows or floods.

4.3. Volume of the fan and the coarse Unit 4

Geophysical investigations using GPR and ERT techniques (Section 3.5) enable us to extrapolate the principal deposit units from

the trenches to the entire fan. The thickness of the fan deposits (without the palustrine Unit 1) ranges between 1.25 and 2.40 m at the apex close to the outlet gorge and decreases to ≤1 m in the north fan area along the Couze Pavin bank. Thicknesses decrease from at least 2.00 m westward down to 1.40 m eastward where both Couze Pavin and the lake outlet have removed the uppermost Units 3, 4 and 5 deposits (Figs. 4, 7). The area of the Gelat fan is c. 86,700 m^2 based on the DSM (Fig. 3B). The fan volume is approximately 139,000 m^3 to 217,000 m^3 with an average thickness of 1.60 m to a maximum of 2.50 m, respectively (Fig. 7A, B). The volume of the preserved fan is 13–37% smaller than the volume of material (220,000–250,000 m^3) that has been removed the outlet gorge and the north rim saddle as shown in Figs. 11, 12 and Table 3; (see Section 6.2 and ESD Table 3, ESD Fig. 6). More material has been removed by Couze Pavin erosion since fan formation (Fig. 4). In contrast, the small volume of the coarse Unit 4, interpreted as a debris-flow deposit, is in the order of 22,000 to 29,000 m^3 if we consider the deposit thickness between 1.0 and 1.30 m in trenches and the lenticular distribution across the four finger-like berms depicted in Figs. 3, 4. A discharge of a few hundred m^3/s would be sufficient to move the coarse Unit 4. Further material was lost through debris flows and/or floods conveyed by the lake outlet and Couze Pavin, as shown by small areas of boulders along the channel down valley beyond the lava dam of the Gelat plain (Fig. 3).

5. Post-eruption evolution: results and hypotheses

5.1. Pavin lake stages and evolution of the lake outlet gorge

Three maar lake stages since the eruption c. 6700 years ago (Fig. 2) are reconstructed by means of the LiDAR DSM from preserved landforms on the maar rim as well as in the outlet gorge towards the Gelat plain (Figs. 3, 4). The profile of the north Pavin maar rim is shown from West to East (1460 m distance) with a DSM 0.5 m contour (Fig. 11A, B). The profile shows that the rim elevation exceeds 1240 m except for the north notch where the lake outlet is located. The 100 m-wide notch, located at the lowest point (c. 23 m above the current

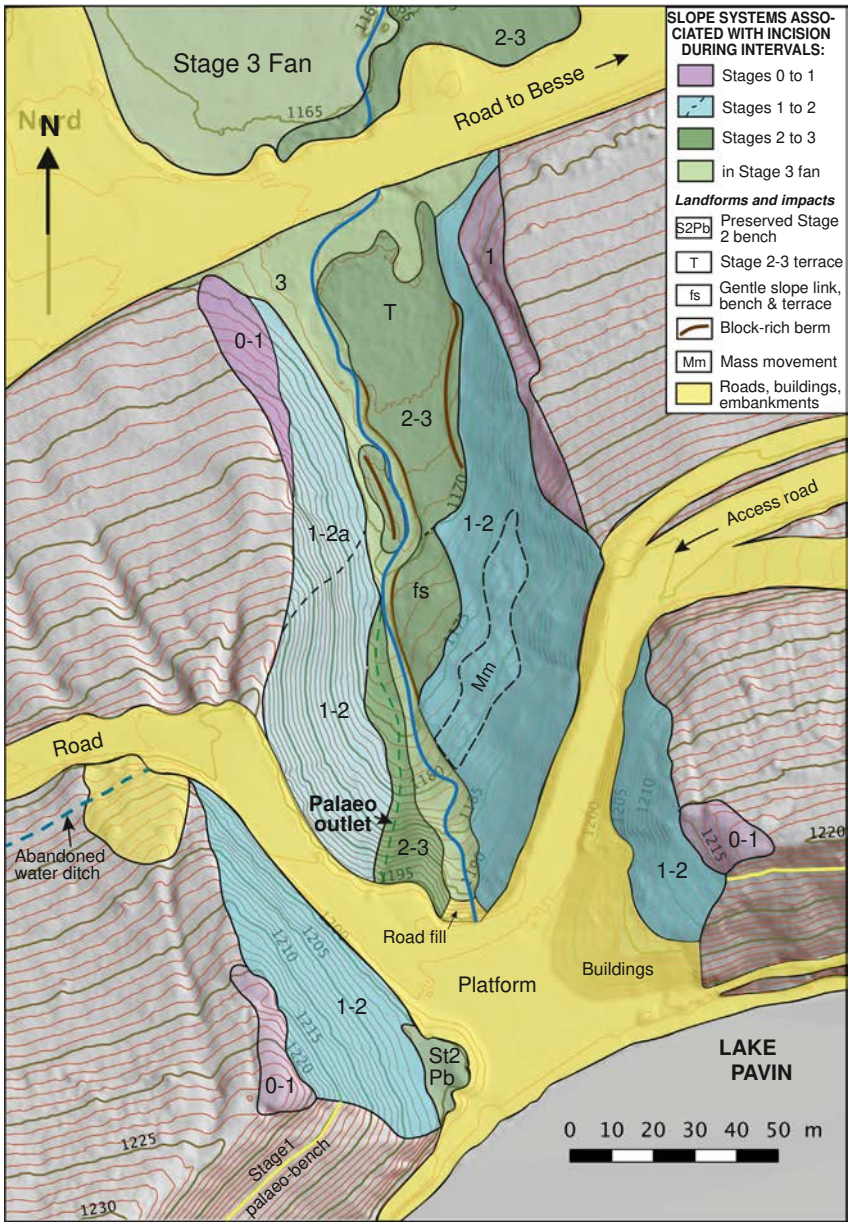

Fig. 12. A. Map of the outlet gorge and lake entrance based on the LiDAR DTM. The three stages 1, 2, and 3 are inferred from the preserved landforms, slopes and landforms along the outlet gorge. **B**. Slope angles are colour coded, five transverse profiles that led us to infer the three stages of outlet formation.

Table 3
Evolution of the volumes of the successive Pavin lakes since the maar formation. Computed input parameters based on Lidar-derived DSM and BRGM DEM. Volumes have been obtained using methods based on trapezoid, Simpson and Simpson3/8 applied to the DSM, which provided identical results (Surfer, Golden software 2015). Symbol meaning: †Annual net water supply is the current value proposed by Jézéquel et al. (2011). †† Beine is a lake terrace straddling the lake shoreline that combines a subaerial bench and a subaquatic accumulation bank.

Stage no. and palaeo-lakes	Elevation, m asl from DSM/IGN	Additional water slice, m	Maximum depth, m without sediment infill	Area, m^2	Total volume m^3	Volume difference, m^3/present lake	Volume difference, m^3/stages	Net supply m^3/year†	Duration for crater water infill, years
3: Current lake	c. 1197 (1196.32)		92	448,970	23,681,250		1,344,300	1,577,880	15
2: Stillstand palaeo-lake preserved bench at north notch	c. 1201 (1200.65)	4	96	464,975	25,025,555	1,344,300	7,613,165	1,577,880	16
1: Highstand palaeo-lake preserved beine†† around maar rim	1215	18	110	518,365	32,638,720	8,957,465	2,640,975	1,577,880	21
0: Maximum rim level at the north saddle lowest elevation	c. 1220	23	115	535,100	35,279,695	11,598,440		1,577,880	22

lake) of the initial rim saddle, coincides also with the narrow dam (c. 65 m) between the current lake shore and the outer north rim slope (Fig. 2B). Using the DSM-derived profiles (Fig. 11A; ESD Fig. 4), the evolution of the saddle and notch has been reconstructed on the basis of the geometry, distribution and extent of the preserved slopes.

5.1.1. Initial maar rim Stage 0

Stage 0 occurred shortly after the end of the eruption. We have reconstructed the immediate post-eruption rim profile before any erosion, which cannot exceed 1220 m (Figs. 2A, 11). Hence, during Stage 0 the lowest point of the initial rim to the north was at ≤1220 m asl (Fig. 11). Following the eruption, the maar has evolved due to runoff, landslide and rock fall on the steep rim slopes, and deltas and turbidites in the lake (e.g., Pirrung et al., 2007; Fepuleai et al., 2018). Based on the observed time lag between historical maar eruptions and crater infill by ground- and spring water (Pirrung et al., 2007), we estimated that a short period of 20–22 years was necessary for the lake to be filled up to 1215 m asl, depending on the amount of water supply according to the annual balance computed by Jézéquel et al. (2011), the permeability of the crater bottom, and fluctuations in groundwater parameters (Table 3).

5.1.2. Lake Stage 1

Stage 1 is based on the existence of the lake terrace (Figs. 3, 7D) at 1215 m asl, 18 m above the current lake level. Stage 1 quickly established once the lake started to flow over the maar rim after the eruption, as the height difference between the lowest point of the saddle (1220 m asl) and Stage 1 did not exceed 5 m and the loose tuff beds were easily eroded (see Fig. 5). Soon after the initial eruption, the highstand lake level settled at 1215 m and remained stable for sufficient time to allow the terrace to develop and the notch to flare out. The profile shown as a pink curve at 1215 m (Fig. 11A) follows the preserved gentle slopes on the higher part of the notch. The terrace at 1215 m was initiated shortly after the eruption, but the lake fell from this highstand shortly before the 5–7th century CE (Table 2, Fig. 2C). As a corollary, the volume of the tuff rim deposit removed and deposited down valley over c. 5000 years shows an erosion rate estimated to be as low as 26–28 m^3/yr (Table 4).

The age of the Stage 1 terrace remains unresolved as dating the bench established in the rim slope is difficult. Three trenches across the bench at site 1 on the NE slope, site 2 on the east slope and site 3 on the south slope (Fig. 2C) have shown colluvium and layers containing gravels and pebbles that formed the beine. Two minimum ^{14}C ages obtained at the site 2 suggest that the bench is older than the 14–15th century (Fig. 2C1, Table 2). These are minimum ages, but the lake terrace initiated well before downcutting from Stage 1 to Stage 2 took place. Once the lake Stage 1 was established at 1215 m, little or no erosion occurred. The proof is that no detrital deposit is intercalated in the palustrine deposit in the alluvial Gelat plain. No mass-flow deposit older than the 7–9th century can be detected in the deposits forming the fan at the mouth of the lake outlet in the Gelat valley (Fig. 7A, B). Weak erosion is also reflected by the composition of palustrine sediment and the stratigraphic position of the gyttja/peat layer intercalated between the reworked maar deposit and the Gelat fan deposits. The top of palustrine units in the marsh to the east of the fan has been dated between the 5th and the 7th century CE (Figs. 4, 7; Table 2). As a result, the Stage 1 terrace was likely abandoned after the 7th century.

5.1.3. Lake Stage 2

Stage 2 corresponds to the bench preserved on the west flank of the notch (dam) at an elevation of 1200.65 m asl, i.e. c. 4.35 m above the current lake level (Figs. 1D, 2B, 5). From Gautié's report (1867), the Stage 2 bench was almost twice as wider as the current bench and slightly higher (at the knickpoint with the west slope of the notch) above the outlet. This bench was the initial point of a weir and lake spillway raised a few meters above a water ditch that was active before the 18th century (see Fig. 7 *in* Miallier, 2020). The spillway was located 10 m west and c. 4.80 m higher than the outlet channel and the lake level in early 20th century, as measured by Bruyant (1909). The elevation difference of c 4.80 m was between the bottom of the abandoned spillway and the active channel at that time (Bruyant, 1909; Eusébio and Reynouard, 1926). The elevated spillway was connected to the former outlet channel west of the current one, while Figs. 2B,5 and 6H show the abandoned channel at the headwall of the outlet gorge.

The poorly preserved c. 1201 m stillstand bench, near the contact between the rim tuff and the RH PDC deposit, indicates that the lithological contact caused downcutting as low as possible during a short period (Table 6, Fig. 11C). This suggests that seepage during Stage 1 occurred at the interface between the maar tuff and the PDC deposit so that when the lake had fallen to the Stage 2 level, the outflow had to cut a new breach in the PDC deposit, potentially by headward erosion and knickpoint retreat. The relatively short interval in which this occurred (a few hundred years in the late Middle Ages versus the ≥1000 year-long drop between Stage 1 and Stage 2, Fig. 11C) reflects the smaller size of the PDC dam.

5.1.4. Interval between Stage 1 and Stage 2

The incision during the Stage 1–2 interval is based on the increase in slope angle observed on the V-shaped notch formed by the outlet (Fig. 11; ESD Fig. 4). The notch east flank, steeper than the Stage 0–1 interval slopes, has been reconstructed as mirroring the west flank (Figs. 11, 12). The notch was cut regularly and without pause because no terrace exists between 1215 and 1201 m asl. The notch slopes cut during the Stage 1–2 interval are steep (30–35°), implying that the

Table 4
Volumes of material removed from the outlet gorge reconstructed during Stages 0, 1, 2 and 3 (see Figs. 5, 12 and ESD Figs. 6, 7), and estimated erosion rates.

Post-eruption evolution	Volume m^3	Volume difference m^3	Computed values using Surfer (Golden Software 2015) and LiDAR DSM (see Fig. 15)	Interpreted from Table 1 See text, Section 6		Stage interval (see Table 6)	See Table 6 for a synthesis and processes
Stage number	E_n-E_0	E_n-E_{n-1}	Trapezoidal, Simpson, and Simpson 3/8 rule techniques	Approximate initial age (years ago)	Estimated av. duration (year)	Average erosion rate m^3/yr	Comment
Stage 0	0			6700	Decades to hundred(s)?		Pristine rim following eruption
Stage 1	c. 138,930	c. 138,930	c. 138,930 to 138,940	1700 to 1500	c. 5000–5200	c. 26–28 between Stages 0 and 1	Long-lasting, slow incision
Stage 2	c. 210,540	c. 71,610	c. 210,540 to 210,545	1300 to 900	A few hundreds?	c. 180–360 between Stages 1 and 2	Moderate to high erosion
Stage 3	c. 248,360	c. 37,815	c. 248,360	800 to 600	Decades to 200?	c. 190–760 between Stages 2 and 3	Short-lasting, high to strong erosion
Present-day lake level	c. 247,910 to 247,460	c. 450	c. 247,460 to 247, 910	160	160	c. 2–3	Very weak erosion due to road containment and controlled outlet at threshold

north rim saddle (in the order of 14.50 m in thickness below the Stage 1 bench at 1215 m) has been incised and a sizeable volume (c. 72,000 m^3, Table 4) has been removed. The 14.50 m thickness results from the 7 m-thick maar tuff deposits resting on the 7.50 m-thick RH PDC deposit (Fig. 5).

Incision between the Stage 1 and Stage 2 benches (1215–1201 m = 14 m) took some time as reflected by the slope system of the gorge and by alluvial deposit forming the fan, which started to push the Couze Pavin river to the north (Figs. 3, 4). The shift of the Couze Pavin River towards the north edge of the plain may have included channel migration back and forth, reflected by the sand-sized and stratified alluvial layers of Unit 2 (Fig. 7). Incision of the lake outlet gorge was relatively slow but repeated, as reflected by the Units 2 (sand sized alluvium) and 3 (gravel and pebble-rich layers) of the Gelat fan (ESD Fig. 3). Units 2 and 3 are younger than the 7th–9th century interval, as inferred from the dated underlying unit 1 (Fig. 7).

Interpretation of the stage 1–2 interval leads to two hypotheses on the Lake Pavin stable surface outlet established at 1215 m asl: either it persisted for 4000 to 5000 years until headward retreat of a knick point initially formed at the downstream limit of the ejecta rim reached the lake barrier, or it was created and maintained by subsurface seepage flow through the ejecta rim. This seepage started to erode the gorge through the rim, yielding the material that forms Unit 2 in the fan. However, in both scenarios, the septum between the lake and the head of the gorge has not thinned to a critical value; rapid collapse and the potentially catastrophic release of water did not occur at Lake Pavin (unless in a limited form as possibly indicated by the Unit 2B deposits being coarser than those of Unit 2A). Instead, as the septum thinned, seepage flow increased, reducing the lake height rapidly but not catastrophically until the final breakthrough. The dam material at the outlet headwall was sufficiently thick (>60 m) and the conglomerate/BAF deposit indurated enough that runaway breaching could not occur.

5.1.5. Interval between Stage 2 and Stage 3

Active incision from Stage 2 to Stage 3 took little time. This is based on the presence of the block-rich berms that form the Unit 4 of the fan underlying the present-day soil of Unit 5 (Figs. 1E, 7). The levees, likely formed by debris flows, are older than the 14-15th century from the dated base of the Unit 5 soil, and much younger than the 9th century, as Units 2 and 3 were deposited in-between Units 1 and 4. We know that the block-rich Unit 4 corresponds to the Stage 2–3 interval (between the bench at 1201 m and the current lake at 1197 m) for two reasons: (1) The upper reach of the gorge shows a channel (palaeo-outlet in Figs. 2, 5, 6G), linked to the Stage 2 bench and cut in the west flank of the dam. This channel was connected through small flattish landforms to a terrace down valley, <1 m above the current outlet channel with levees of blocks on both sides (Fig. 5, ESD Fig. 5). (2) The cobbles and boulders of Unit 4 belong to Monts-Dore lavas and/or the conglomerate, indicating that the gorge had already cut down through the rim and the notch long before Stage 3 (Fig. 11). The coarse material of Unit 4 also includes ballistic boulders on the steep slopes of the gorge, removed by debris flows or floods. Relatively fast erosion during the Stage 2–3 interval has removed a volume of c. 38,000 m^3 (Table 4). Eventually, the northward migration of the Couze Pavin channel 250 m across the Gelat plain resulted from the prevailing debris supply from the lake outlet, as witnessed by the coarse debris-flow Unit 4 and finger-like berms. The presence of the boulder Unit 4 in the fan that correlates with the timing of the Stage 2–3 lake level fall suggests that this drop of c. 4 m was accompanied by a debris-flow/flood event that resurfaced the fan. Waning flow then incised the debris-flow deposit to produce the four finger-like berms.

5.1.6. Final growth of the Gelat fan and lake at Stage 3

Stage 3 is the modern lake level at c. 1197 m (green line, Fig. 11), which coincides with the top of indurated conglomerate. The present-day profile of the north part of the maar rim has been reconstructed before any human impact (Fig. 1B; ESD Fig. 4). The present-day, constructional beine has been associated with the current lake level at least since the end of the 18th century according to descriptions made by Legrand d'Aussy in 1794–1795 (*in* Miallier, 2020). Once the river was pushed to the north edge of the Gelat plain, incision took place, as the channel has cut 2 to 3 m below the fan top (Fig. 4). This 2–3 m-deep channel includes the lowermost, inset constructional terrace about 1.5 m thick. The incision deepens to 3 to 4 m towards the east end of the Gelat plain as the regressive erosion took place at the lava flow dam downvalley (Fig. 3). The incision initiated after the minimum age of the base of the Unit 5 soil, i.e., prior to the 16th century (Fig. 7, Table 2).

5.1.7. Stable lake level over the past 160 years

The variations of the lake level over the past three centuries have been summarized by Miallier (2020). The lake level has remained

around 1197 m since at least 1860. Small variations in lake level were recorded, but did not exceed one meter. Lake level changes were caused by exceptional rainfall and drought, and human impacts on the outlet. The constructional beine, now under water near the current lake level at 1196.32 m asl, has remained stable despite works for tourism and fishing including a round-the-lake trail, a pontoon and jetty for small boats, and a platform covering the outlet channel.

5.2. Variations in Lake Pavin water volume since the maar eruption

Fig. 11A, C summarizes the different lake stages. Based on the DSM reconstructed profiles (ESD Fig. 1), the surface area and volume of the water bodies have been computed for each of the stages that corresponded to three lakes (Table 3). Such figures have been inferred from the present-day morphology of the crater (known from multibeam bathymetry, BRGM, 2011), but we did not take into account sediments at the lake bottom and crater widening due to erosion and cliff rock fall. Results shown in Table 3 have used the current hydrological balance proposed by Jézéquel et al. (2011). The drop between the lake 1 at 1215 m and the lake 2 at c. 1201 m implies a loss in water volume of c. 7.62 million m^3. This water volume loss probably occurred over a long period of 200 to 800 years, as discussed in Section 6.2 (Table 4). The volume of water lost between the Stage 2 and 3 lakes was six times smaller (1.34 million m^3, Table 3), but spanned a shorter interval (maximum of 200 years; Table 4).

6. Discussion

6.1. Maar lake break-out and flood

Lake overspills and subsequent mass flows have rarely been described at maars, compared to other crater lakes on polygenetic volcanoes (e.g., Ruapehu, NZ) and in calderas (e.g., Taupo, NZ) (Manville, 2010, 2015). But maar lakes contain substantial volumes of water (Tables 1, 3, 5), which can be partly released when lake outlets breach shallow and narrow rims, and the resulting floods or lahars affect people living downstream (e.g., Lake Albano in 398 CE; de Benedetti et al. (2008)). Table 4 displays rare examples of unstable maar lakes and provides some comparison with other volcanic lakes, in particular 'type III' crater lakes. Manville (2015) established a clear distinction between three types of volcanogenic lake break-outs: Type I phenomena sourced within the lake basin as a direct or indirect consequence of subaqueous or subaerial volcanic activity. Type II floods from volcanic lakes triggered by volcanic activity, including induced breaching of the lake rim. Type III floods from volcanic lakes with a non-volcanic cause, termed passive lake break-out by Manville (2015). The Pavin maar provides an example of type III passive lake break-out and floods without a volcanic cause (Table 5).

6.2. Inferring lake outlet incision rates from the gorge slope system and fan deposits

To quantify the evolution of the outlet gorge and estimate the volumes of material removed, we have used the DSM of the gorge (ESD Fig. 6) together with a 3D print-out model of the north rim saddle, notch and outlet gorge (ESD Fig. 7, ESD Table 3).

Firstly, we computed the volume of material removed from the outlet gorge by extracting the present-day DSM topography of the gorge (ESD Fig. 6D) from the topography of the gorge filled with the removed material (ESD Fig. 6A). The 'missing' volume, which was removed from the gorge, amounts to 250,000 m^3, comparable with the 225,000 m^3 amount derived from the physical 3D-model (Table 4; ESD Fig. 7; ESD Table 3). This amount is consistent with the bulk volume of the fan, i.e., 139,000 to 217,000 m^3 (see Section 4.3), the more so when we take into account: (i) the material flushed away through the Couze Pavin, (ii) the degraded north and east areas of the fan, and (iii) the Couze Pavin channel inset ≥ 2 m in the fan surface (Fig. 4).

Secondly, we depict three stage intervals during which the north rim saddle, notch and the outlet gorge were eroded based on the DSM and 3D-model (ESD Figs. 6B, C, D, and 7), enabling us to estimate eroded volumes and incision rates (Tables 4, 6).

1. The north saddle was flared out as a broad and shallow valley between Stages 0 and 1. Gentle slopes < 15° preserved high on each side of the notch witness to the shallow opening of the narrow saddle (Figs. 11C, 12, ESD Fig. 6A). The physical 3D-model yields a maximum volume of about 2000 m^3 for the Stage 0–1 interval, while the DSM-based computation yields a maximum of 139,000 m^3 of material removed (Table 5; EDS Table 3). The physical 3D-model and the DSM computation pursue different objectives, so the volume estimates are quite different: the model captures snapshots of the erosion processes at the onset of the intervals, whereas the DSM computed volume records the erosion amount at the end of each interval. Between Stage 0 and 1, the average erosion rate remained low (26–28 m^3/yr) as the interval may have lasted 5200 years (Table 4).
2. Erosion took place during the Stage 1–2 interval. The volume of material removed was c. 72,000 m^3 (DSM, Table 4) to 116,000 m^3 (physical model, EDS Table 3). The erosion rate was moderate to high between 180 and 360 m^3/yr (Table 4). We subdivide two sub-stage intervals: 2a. The notch cut down the previous Stage 1 wide and shallow valley at the lowest rim location (ESD Fig. 6B), as suggested by the notch steep slopes > 25° (Fig. 12; ESD Figs. 6, 7). 2b. Downcutting progressively shifted to the west side of the dam where the lake 2 bench and weir are preserved (Figs. 6H, 12; ESD Fig. 6C). The shift in incision to the west side of the notch can be explained by: (i) the unconformity between the RH PDC deposit and the volcaniclastic conglomerate, and (ii) gullies cutting down the outer rim slope prior to Stage 2 (Figs. 1C, 3).
3. Downcutting removed a large part of the Stage 2 bench (c. 38,000 m^3) down to Stage 3 (168,000 m^3, EDS Table 6), so the erosion rate accelerated from 190 to as much as 760 m^3/yr (Table 4), coinciding with the coarse Unit 4 deposit of the fan (Fig. 6). Incision shifted to the east side of the dam where the outlet is now located (ESD Fig. 6D). This shift may be due to N10E fracturing and the unconformity between the loose RH PDC deposit and the indurated conglomerate located on the east side of the outlet (Fig. 6B).

6.3. Formation of the lake outlet channel

6.3.1. Geomorphological and hydrological mechanisms

The geomorphological and hydrological mechanisms leading to the formation of the outlet gorge include: (1) erosion by an overflow channel; (2) piping or seepage erosion within the permeable tuff and the weathered and fractured conglomerate forming the natural dam, and; (3) headward erosion by the Couze Pavin river downstream of the lake.

To explain the formation of very short (<200 m), narrow (<60 m), steep (18%) and concave-shaped valleys like the Pavin outlet is challenging because such gorges lack an upstream channel and an extensive catchment providing enough discharge. Using laboratory experiments and numerical hydrologic modeling, Marra et al. (2014) explored the processes involved in the formation of short valleys without large catchments in sediments, to unravel the source of sufficient erosional power for incision. We correlate the slope system and terrace of the outlet gorge (Figs. 5, 12) to the specific landforms exhibited by valleys emerging from the first mechanism, groundwater seepage and headward erosion based on their experimental tests. After channel initiation, groundwater flow converges towards the valley head causing headward erosion of the valley. Estimate of the formative timescale suggests that short valleys form relatively slowly as fluvial transport takes place in a channel much smaller than the valley. Supplied by groundwater seepage, small fluvial channels within the valley have constant dimensions during the valley formation.

Table 5
Reported lake outbursts from maar lakes, and volcanic crater lakes for the purpose of comparison. Characteristics and hypothetical triggering mechanism(s). Symbol meaning: † Hazard type after Manville (2015). †† We report how Chassiot et al. computed the volume of water released from the lake at around 600 CE, but the surface of the Stage 1 lake was 13% larger with a level 14 m higher than the current lake.

A. Maar lake outflows and/or gas outburst, and lake mass-flow break-out

Maar/crater lake name, location	Lake outflow event & type†, approximate dates	Lake volume $\times 10^6 m^3$	Dam type, height, m/ Breach depth, m	Mass flow type and occurrence	Flow runout distance km	Mass flow volume $10^6 m^3$	Maximum discharge Q_s m^3/s	Effects or impacts	Triggering mechanism: hypothetical or reported	References
Lake Pavin, Auvergne, France	Long-term: between <4720 BCE and 600 CE Short-term: between 800 and 1400 CE	32.64 25.03	Rim Dh 20, Bd 9 Rim Dh 6, Bd 5	Floods and hyperconcentra-ted flows Debris flows	?	Max. 8.96×10^6 (long-term) Max. 1.34×10^6 (short-term)	?	Formed a fan; Produced floods and debris flow(s), impacts unknown	Seeapge and lake overflow: Subaquatic landslides? Exceptional rainstorm?	Thouret et al., 2016; This study; G. de Tours *in* Vernet, 2013
Pavin	600 CE 1300 CE	3.96 *(0.44 $km^2 \times 9$ m)*††		«Catastrophic flash flood»		«water discharge» 3.96×10^6 No estimate	1.5×10^3 (reconstructed)	Flood down valley to La Villetour hamlet of Besse town	Subaquatic landslides linked to regional earthquakes	Chassiot et al., 2016a, 2016b, 2018; Lavina and Del Rosso d'Hers, 2009
Godivelle d'En-Haut	Late Glacial, LGM	2.74	Rim Dh 21 m Bd 7 m	Unknown	c. 0.72	Fan 0.017 $km^2 \times 2$ m= 34,000 m^3	?	Fan down valley Flood	Lake overtopping?	Juvigné, 1992 This study
Nyos, NW Cameroon	21 August 1986		Rim Dh 40	Water jet, CO_2 gas outburst (1.6 million tons), waves, hydrothermal jet				1746 fatalities, 8000 livestock; 874 injured, 4434 displaced	Limnic eruption Roll over Supply of magmatic CO_2 from lake bottom	Sigurdsson et al., 1987; Kling et al., 1987; Kusukabe, 2017
Monoun, W Cameroon	15 August 1984		Rim Dh 30	Water wave attained 5 m in height				37 fatalities	Limnic eruption	Sigurdsson et al., 1987; Kusukabe, 2017
Albano, Colli Albani, Italy	Overflows 5800, 2400 yr BP; 398 BCE level rise 1827, 1929		Rim Dh 150	Overflow avoided. by first ever dug tunnel. Lahar(s). Anomalous degassing	15–18 Ciampino plain towards Rome			Tunnel dug by Romans in 394 BCE. Degassing linked to seismic activity	Lake level overflow; Repeated degassing. Tunnel keeps level 70 m below	Anzidei et al., 2007;De Benedetti et al., 2008; Funiciello et al., 2003; Riguzzi et al., 2008
Monticchio Grande and Piccolo, Mt. Vulture, Italy	LGM 1770, 1810 CE LPM 1820		Rim LGM Dh 25 LPM Dh 10	Gas outbursts		3–6 m high water column		No fatalities Dead fish		Cioni et al., 2006; Caracausi et al., 2013; Spicciarelli and Marchetto, 2019

B. Other volcanic lake dam failure and mass flow break-outs for comparison

Maar/crater name, location	Event approximate dates and type†	Lake volume $10^6 m^3$	Dam type, height, m/Breach depth, m	Mass flow type and occurrence	Mass flow runout distance, km	Released water/Mass flow volume m^3	Maximum discharge Q_s m^3/s	Effects or impacts	Triggering mechanism: hypothetical or reported	References
Ruapehu crater lake, New Zealand	2007 Type III	10	Tephra Dh 6.4 Bd 6.4	Debris flow Lahar	>35	1.0×10^6	530	Distal flooded areas	Lake dam break-out	Manville and Cronin, 2007; Schaefer et al., 2018; Massey et al., 2014
Ruapehu crater lake, dam failure	1953 Type III	10	Ice/tephra Dh 20 Bh 8	Lahar	<35	1.8×10^6	350	151 victims Train	Lake dam break-out	Manville, 2004
Te Maari crater, Tongariro, New Zealand	13 October 2012 Type III	0.005	Debris ava-lanche dam Breach 59 × 12	Debris flow Lahar	4.5	57×10^3 Sediment $>57 \times 10^3$ water		No fatalities	6 August 2012 eruption and debris avalanche Tee Mari vent	Walsh et al., 2016
Parker, Philippines Crater lake	1995 Type III		Rim	Flood		3×10^7		>60 victims	Crater lake dam failure	Manville, 2015
Santa Maria, Guatemala	Valley lake Nimá1 1978 Type		Impounded valley	Lahar						Manville, 2015

Table 5 (*continued*)

B. Other volcanic lake dam failure and mass flow break-outs for comparison

Maar/crater name, location	Event approximate dates and type†	Lake volume $10^6 m^3$	Dam type, height, m/Breach depth, m	Mass flow type and occurrence	Mass flow runout distance, km	Released water/Mass flow volume m^3	Maximum discharge Q_s m^3/s	Effects or impacts	Triggering mechanism: hypothetical or reported	References
	III									
Pinatubo, crater lake, Philippines	Bucao River 10 July 2002 Type III	160	Caldera rim Dh 175 Bh 23	Post-eruption largest lahar		6.5×10^7	3×10^3			Lagmay et al. 2007 *in* Manville, 2015
Castle Lake, Mt. St-Helens, USA	1980 debris-avalanche dam Type III			Spillway						Spicer and Mosbrucker, 2017
Kelut, crater lake, Indonesia	1875 Type III		Rim	Lahar	27–37	3.8×10^7		10,000 victims in 1586; 5160 in 1919 Extensive farmland	Lake overflow, Eruption; Tunnels dug in 1922–1926	Suryo and Clarke, 1985; Thouret et al., 1998

The second mechanism is crater-lake overflow; a body of water overtops the rim of the lake, followed by rapid incision of the rim and valley formation, which depends on the rate of knick point retreat. The size of the Pavin outlet gorge does not change substantially from the narrow (30–40 m) headwall to the 50–60 m-wide mouth. The final channel width is smaller than the relevant channel width during most of the event.

At Lake Pavin, the narrow outlet channel with a low discharge, associated with several springs along the outlet banks, advocates seeping groundwater and lake leakages. The strong contrast between the channel and the gorge dimensions together with the mass-flow deposits of Unit 4, however, advocates short episodes of crater-lake overflow (Figs. 1C, 7B). These observations allow us to propose two events: (1) groundwater seepage and headward erosion of the outlet prevailed over the long interval between Stages 1 and 2; (2) crater-lake overflow prevailed over the short interval of erosion between Stages 2 and 3. Valleys cut by a lake overflow develop quickly as increased discharge enhances erosion.

6.3.2. Outlet discharge fluctuations

Discharge fluctuations should be considered to explain the formative timescales of the gorge.

1. Lake Pavin was long perched at 1215 m after the initial eruption until at least the 5th century, i.e. at least 5000 years. Over the Stage 0–1 interval, incision was weak, as witnessed by the lack of alluvial deposits in fan Unit 1. Low discharge of the initial outlet was associated either with water leakages at the base of the lava cliffs covered by the Stage 1 lake or with a dry/cool climate prior to the Early Middle Ages. The outlet discharge was also low because evaporation and leakage of the lake were enhanced at this time; the extensive Stage 1 lake at higher elevation was much less confined below low rims than the current lake. As a result, the outlet gorge profile was less concave than the present-day gorge at the beginning of Stage 1 when the Couze Pavin was reworking the maar deposit. The gorge profile may not have changed during Stage 1 due to low discharge and reduced transport, when the Couze Pavin-Gelat did not record any substantial detrital material from the lake outlet.
   Evaporation acting on the highstand lake at 1215 m asl, 13% more extensive than today (Table 3), may have been enhanced during the mid-Holocene climatic optimum over the first 1600 years of the early Lake Pavin (i.e., between c. 6700 and 5100 years ago). If the average temperature was 1 to 2 °C above the current one in the region (Macaire et al., 2010), evaporation increased by about 10 to 15% of the current value (320 ± 150 m^3/day; Jézéquel et al., 2011), if other parameters were kept constant. However, evaporation was largely compensated by increased rainfall during the slightly warmer and humid Atlantic period. Moreover, enhanced evaporation from the early Pavin lake may be over-estimated, because snow/ice cover at the lake surface and across its watershed prevents evaporation during at least four winter months. Hence, enhanced evaporation may have influenced water loss from the early lake between 6700 and 5100 years ago, but it could not lower substantially the thousands-long highstand lake and did not match the total loss of water volume of 7.62 million m^3 within the c. 1000 year-long Stage 1–2 interval (see Tables 3, 6). Palaeo-ecological data from sediment cores extracted at comparable altitude in the region points to limited temperature and humidity fluctuations following the Atlantic optimum, while oceanic and wet climatic conditions existed in the French Massif central over the past 2670 years, thus including the Stage 1–2 interval (e.g., Macaire et al., 2010; Lavrieux et al., 2013).
1. Faster incision, which started after the 9th century (on the basis of the fan Units 2 and 3), suggests increasing discharge and/or runoff caused by receding forest due to developing settlements and farming (Stebich et al., 2005; Schettler et al., 2007). Analyzing a 19 m-long sediment core drilled from Lake d'Aydat, 19 km NNE of Lake Pavin, Lavrieux et al. (2013) demonstrated that many floods started after the 9th century and increased between the 11th and 15th century, which produced many detrital layers intercalated in the lake sediment. Vernet (2013) also reported large-scale detrital events over the Middle Age in the basin of Limagne 10 km NE of Aydat, although anthropogenic impacts declined between the mid-14th century and mid-15th century. We suggest that the fast incision of the Stage 2–3 interval prior to the 14th century was triggered by heavy rainstorms, flood events, and perhaps human impact.
2. Following the 15-16th century, the outlet discharge abated due to reduced rain and perhaps water intake from the lake. This water intake was abandoned during the 19th century, as mentioned by Eusébio and Reynouard (1926).

6.4. Hazards

6.4.1. 'Extreme lake spillovers' in published limnological investigations of Lake Pavin

Following Henriet (2009), who first described a subaquatic terrace 40 m below present lake level in the NE sector and landslips on its edge, Chapron et al. (2010, 2012) conducted a detailed geophysical survey of the lake and attributed landslip scars on the front of the terrace and mass wasting deposits (MWD) to events triggering lake waves and spillovers. From analysis of lake sediment cores, Chapron et al. (2010, 2012) postulated that a subaquatic landslide occurred between 580 and 640 CE. Their key evidence is a sedimentary sequence from the PAV10E core, the facies of which ranges between that of diatomite (i.e. deep lake facies) and shoreline (i.e. shallow environment).

Table 6
Synthesis of lines of evidence and hypotheses for reconstructing the post-eruption evolution of the Pavin maar and lakes. See Discussion Section 6 for details. Literature*: Chapron et al. (2010, 2012); Chassiot et al. (2016a, 2016b, 2018). ** Lavina and Del Rosso (2009).

Post-eruption evolution Stage and Interval	Preserved landforms and/or deposits Estimated incision rate and pause				Deposit type	Estimated initiation age, years (Table 5)	Estimated average duration (years)	Lake level drop, m	Process and/or mechanism (See Discussion, Section 6)		Lake level and events *from the literature**
	On rim	In outlet gorge	In fan	In Gelat valley			This study (Table 5)	This study	Observed or inferred	Hypothetical	
STAGE 0 1220–1215 m	Pristine ridge top	Gentle rim slopes			Maar tuff	c. 6730 ago	Several tens, 100?	0	^{14}C dated tuff deposit		
INTERVAL between Stages 0 & 1	Broad, shallow, valley	Slow lake overtop-ping	Middle terrace	Reworked tuff deposit	Reworked tuff	Well before 6000 yr ago	100 to a few 100 s?	5 (max)	Runoff	Slow lake overtopping, low discharge	
STAGE 1 Palaeo-lake highstand 1215 m	Bench +c. 18 m	Gentle slopes	Palustrine deposits	Palustrine deposits	Gyttja, peat	Between 800 BCE and 500 CE or 900 0CE	4000 to 5000	0	Pause Extensive and voluminous palaeo-lake 1	Dry and warm? Enhanced evaporation and leakage	Diatom-rich deposits
INTERVAL between Stages 1 & 2	V-shaped valley incision	Slow incision	Alluvial Unit 2	Alluvial deposits	Alluvium	Between c. 500 BCE and c. 500–700 CE	1000 to maximum 1200	14	Groundwater seepage Rainstorm, Human impact	Outlet downcutting, higher discharge Wet period, early Middle Ages	6, 9 or 13 m drop, 600 CE 'extreme event' (Earthquake trigger*)
STAGE 2 Palaeo-lake c. 1201 m	Bench +c. 4.30 m	Cut in Rioubes-Haut PDC	Alluvial deposits	Alluvial deposits	Alluvium	1100–1400 CE?	100 to 200 s?	0	Pause in incision	Stillstand coincides with Rioubes-Haut PDC deposit	Diatom-rich deposits (continue today)
INTERVAL between Stages 2 & 3	Natural spillway	Fast incision, steep slope system	Torrential Unit 3	Stream-flows, floods	Hypercon-centrated flow, flood	Prior to 1400–1600 CE	Several tens to 200?	4	Unit 3 flows Repeated, heavy rainstorms?	Lake overflow High discharge Dam lithological unconformity	c.1300 CE 'extreme event' (Earthquake trigger*)
STAGE 3 Final fan growth	Top of natural dam	Palaeo-outlet, terrace	Fan berms, Unit 4 debris flow	Flood and perhaps mass flow	Boulder, cobble and pebbles	Prior to c. 1700 CE (c. 1600 CE?)	100 to 200?	0	Unit 4 DF; Fan growth; repeated, heavy rainstorms	Detrital input Human impact Dam lithological unconformity	
Since 16th or mid-18th century	Gorge headwall	Terrace Boulders in channel	Unit 5/soil	Incision, then low terrace	Sand, gravel	c. 1515 CE? 1770–1790?	250–420?	0–1	North & east fan areas incised	Drought	2-m level rise or 4 m drop: human impact
Present-day lake c. 1197 m	Small gullies, runoff	Small, controlled channel	Slight incision	Slight regressive erosion	Sand	Mid-19thC lake & outlet outlet control	Minimum 160	Submerged beine <1 m	Fan planed by agricultural practices		

Chapron et al. (2012) recorded the PAV10E core as under 17.5 m of water, whereas the nearshore facies and sequence are now located about 26 m under the surface. From the contrast in facies, the authors infer that the lake level has suddenly dropped by 8.5 m, rounded to 9 m (=26–17 m) in the later publication. Later, Chapron et al. (2012) reduced the drop range to 6.5 m to account for a postulated lake level rise of 2 m due to 'human infrastructure' around 1855 at the outlet. The range of lake level drop fluctuates in publications between 6.5 m (Chapron et al., 2012), 9 m (Chassiot et al., 2018) and 13 m (Chassiot et al., 2016b). This discrepancy was noted by Miallier (2020) who demonstrated, on the basis of engineer surveys and historical reports, that the claimed rise of 2 m in 1855 and the lake level drop of 4 m at the end of the 18th century never happened.

Chassiot et al. (2016a, 2016b, 2018) expanded the significance of such MWDs as lake wave and overspill triggers, with subsequent mass flows, and called them 'extreme' events. According to sedimentology and chronology of subaquatic infill deposits (Chapron et al., 2010, 2012; Chassiot et al., 2016a, 2016b, 2016c, 2018), two 'extreme' events occurred around 600 CE and 1260–1300 CE. Chassiot et al. (2016c, 2018) attributed the MWDs to the intensity of regional earthquakes based on concomitant MWDs detected in several subaquatic cores extracted from maar and non-volcanic lakes. This assumption is controversial, and the principal flaw is the following: peak ground acceleration (PGA) measured in unconsolidated subaquatic sediment is poorly known, yet this is a key factor for triggering mass movements and liquefaction (e.g., Douglas, 2003). Moderate to heavy damage only occurs at 0.3–0.6 g (intensity VII–VIII) for shallow earthquakes (<15 km deep) (Wald et al., 2005). Such intensities and damage near Lake Pavin were never reported from historical earthquakes.

Chassiot et al. (2016b, 2016c) increased the range of lake level drop to as much as 13 m to account for a further drop of about 4 m that would have occurred at the end of the 18th century. The authors assigned this lake drop to the subaquatic landslide that occurred about '600' CE. This landslide would have triggered waves that damaged the natural dam and produced lake overspills. The age of the first identified subaquatic mass movement 'around' 600 CE (Chapron et al., 2010) was actually oversimplified from the ^{14}C ages in recent publications: the ^{14}C age 1430 $\pm$ 21 BP (Chapron et al., 2010), calibrated as 610 $\pm$ 30–60 CE (1–2 σ) and compatible with the 550–670 CE interval, should not be oversimplified as '600' CE. Chassiot et al. (2016b) further claimed that this 'extreme' event 'around 600 CE' would have triggered lake overspill of 3.96 million m^3, but from Tables 3, 5, we suggest that the volume of water was at least 34% smaller and emptied after the Stage 2–3 interval over tens to one hundred years (Table 5). The estimates in water volume loss at 3.96 million m^3 and peak discharge of 1500 m^3/s (Chassiot et al., 2016c) are exaggerated in the light of documented crater lake failures, voluminous lahars, and much longer channels, such as the Mt. Ruapehu 1953 and 2007 events (Table 4) to which Chassiot et al. compare the 'twice larger 600 CE Pavin outburst'. The 2007 Ruapehu Crater lake lahar peak discharge during the tephra dam failure was c. 530 m^3/s, *not* 1500 m^3/s (Manville and Cronin, 2007).

Following Henriet's findings (2009), Lavina and Del Rosso d'Hers (2009) announced that a "catastrophic debris flow" occurred along the Couze Pavin as far as 10 km down valley from Lake Pavin. They further claimed that bones and pottery associated with debris-flow deposits were found near the river in La Villetour, a hamlet of the town of Besse about 3.5 km down valley from Lake Pavin. Their findings are controversial since the bones and pottery come from a pit adjacent to a chapel; the objects have not been properly dated and their relationship with the postulated debris-flow deposits have not been demonstrated (e.g., BRGM, 2007). Without any evidence, Chassiot et al. (2016b) linked the 'outburst flood' claimed by Lavina and del Rosso to a lake wave-triggered overflow by describing an 'outburst flood' deposit along the Couze Pavin. More recently, Chassiot et al. (2018) assigned the sedimentological change observed in the sediment core PAV08 to an event indirectly dated at 1300 CE on the basis of regional earthquake intensity. The c. 1300 CE event is represented by a large MWD in the central basin (RDL10 in PAV12) that the authors believe was 'certainly connected' to a large slide scar clipping the edge of the subaquatic plateau, and responsible for 'violent waves'. We interpret MWDs' role the other way around. As one of the dated MWDs (c. 1300 CE) is close to the inferred age prior to the 14th Century of Stage 2 lake level fall in this study, the rapid lake level drop may have triggered the MWDs by lowering the hydrostatic confining pressure on the lacustrine sediments, rather than the MWDs triggering the lake level falls due to tsunami waves causing erosion and outflow of the outlet.

The small-volume debris-flow deposit (Unit 4 DF, Fig. 7) in the Gelat fan, and the absence of substantial DF deposits along the Couze Pavin down valley (Fig. 3) do not support the idea of 'catastrophic flash floods downstream in the valley'. The thickness range (0.25–0.75 cm) of the 'outburst flood deposit' (Fig. 12B *in* Chassiot et al., 2016b) cannot yield a large volume, let alone a 'catastrophic' flood event. The authors reported a maximum age of 1765 $\pm$ 55 cal BP, i.e., 130–240 CE for the upper part of the eroded peat underlying the base of the 'outburst flood deposit'. These dates contradict the idea that the outburst flood deposit resting on the peat layer is a result of the postulated '600 CE extreme event'. To attribute the eroded peat to this 'extreme event', the published 1765 cal BP date would mean that a slice about 70 cm thick, representing about 400 year-long peat growth (e.g., Lavrieux et al., 2013), would have been eroded away, which is improbable given the climate conditions at that time and the limited erosion power of a small-volume debris flow.

Exploring the historical lake 'misbehaviour', Meybeck (2016a, 2016b) raised the issue of two limnic or hydrothermal events and subsequent Lake Pavin overspills in 1783 CE and 1936 CE. Most of his lines of evidence stem from stories by visitors and legends. Chassiot et al. (2016c) related two layers in the PAV08 core with lower TOC and HI values but higher iron content, and dated at 1700 CE $\pm$ 15 and 1915 CE $\pm$ 5, respectively. They relate these dates to visual descriptions of "unusual behaviour of Lake Pavin water" in 1783 CE and 1936 CE reported by Meybeck (2016a). The published ^{14}C dates cannot correspond to visual description dates even with 2 σ error range. Aware of the discrepancy, Chassiot et al. (2018) attributed the time gap to a lack of accuracy in the age-depth model of the PAV08 core.

6.4.2. Failure of maar rim dams

Dam failure at maar rims can be triggered by five mechanisms (Jouhanneau et al., 2001; Bonelli et al., 2007; Manville, 2015; Tchindjang, 2018): (1) Mass movements induced by seismic ground acceleration and liquefaction; (2) Phreato-magmatic eruption near the dam; (3) Regressive mechanical or linear backward erosion following a flood affecting the downstream portion of the dam; (4) Cavity collapse at the dam base or top due to chemical erosion, subsidence, and seepage; (5) Failure due to seepage (piping flow) initiated by headward erosion of a pipe, often accompanied by collapse of the pipe roof to form a retreating amphitheater-headed gully, until only a thin septum of dam material remains that is pushed over by the weight of the lake water, followed by potentially runaway breach erosion.

Mass movements of crater walls trigger waves and seiches across lakes: Wagner et al. (2003) reported one example of an outlet flood from a volcanic lake triggered by a landslide of 150,000 m^3 in 1999, from the crater walls of the Quaternary Kasu tephra cone in the highlands of Papua New Guinea. The landslide displaced 5–10% of the lake's volume, triggering a 15 m-high wave that overtopped a low point on the crater rim, killing one person. Continental lake tsunamis or seiches of volcanic lakes in Nicaragua have been described by Freundt et al. (2007). Two closest non-maar examples of lake break-out lahars and floods (Table 5; Manville, 2015) are the Kelut (Java) 1875 cold lahar triggered by the crater rim failure and the Parker (Philippines) 2002 rim breach and flood (Table 5).

Mechanisms described above have not led to the Pavin dam failure. By analogy with observed breaching of natural dams (and the 2007

Ruapehu Crater Lake dam; Manville and Cronin, 2007), failure initiated by overtopping occurs when surface flow creates a knickpoint at the downstream end of the dam, which then migrates upstream by knickpoint retreat until it reaches the lake, triggering dramatically increased outflow and runaway growth of the breach. The dam duration then depends on a number of factors: here, the short (125 m) and steep (18%) downstream dam face, and contrasts between erodible dam material at the top and less erodible material at the base, are negative factors, but the overflow discharge remains low. This factor contributed to safety in the current conditions.

6.4.3. Potential instability of the Lake Pavin dam

The fate of Lake Pavin natural dam has not raised major concern among scientists who have investigated potential limnic eruptions and Nyos-type gas outbursts. In contrast, Lake Nyos focused scientist attention on the potential failure of the shallow rim dam, following the lethal gas outburst (Jouhanneau et al., 2001; Kusukabe, 2017). Pavin's dam is impounding the upper quarter of the 23.7×10^6 m^3 lake less than 200 m from the Couze Pavin valley and 3.5 km from the nearest settlements.

Based on two BRGM reports (2011) and field investigations (Fig. 5, 7A, B), the geotechnical characteristics of the rim and dam deposits point to relatively mediocre properties, although geophysical investigations did not show evidence for large slope instability: (1) the loose and permeable tuff is erodable as beds lack cohesion (C'_r 0 KPa) and have low to average residual shear strength ($21.9 < \Phi'_r < 44.5°$). (2) The ash-and pumice-rich RH PDC deposits exhibit a near-0 residual cohesion and a low residual shear strength (30°). (3) The underlying conglomerate, though massive, cohesive and indurated, is weathered and fractured, allowing water leakage from the lake. Lake leakage is known to occur c. 9 m (below the lake platform) near the culvert and at greater depths along the dam downward face. (4) Although the low residual shear strength (21–33°) of the indurated BAF deposit is comparable to that of overlying deposits (BRGM, 2009), the higher BAF cohesion (C'_r 13–40 KPa) would explain why the wide dam downward face is relatively resistant.

Compared to Lake Nyos, Lake Pavin whose volume (23.70 million m^3, Table 1) is 7.6 times smaller, is buttressed by a natural dam more narrow, smaller, and shorter than Lake Nyos' dam. A geomorphological dimensionless index has been used after Ermini and Casagli (*in* Capra, 2007) to classify natural dams and estimate their stability. At Lake Pavin, the relationship between the maximum height of the dam Hd = 23 m (Fig. 5), the watershed area Ab = 0.81 km^2 (Table 1), and the dam maximum volume range Vd = 187,000–509,000 m^3 (with L = 125 × W = 65–177 × H = 23 m), suggests that the characteristics of the Lake Pavin dam lie within the safe range, compared to Lake Nyos for example (Hd = 52 m, Ab = 8 km^2 and Vd = 8,112,000 m^3) that impounds a considerable water volume of 180 million m^3 (Table 1). However, Lake Pavin's dam long-term stability may be threatened by three processes: (1) groundwater seepage and piping through low cohesion, permeable pyroclastic deposits. Groundwater seepage from the lake, at work within the RH PDC deposit, supplies Fe-rich springs near the culvert north of the dam and along the outlet channel; (2) The 0.7-m height difference between the lake level and the dam top, which could lead to overflow if a rockslide triggered a seiche, and; (3) Knick point retreat is probably acting within the conglomerate inset in BAF (Fig. 5).

The dam and access to the lake were reshaped after 1950. The top of the conglomerate, armoring a 10 m-high headwall cliff, was flattened and the front buttressed by a road embankment. The lake dam has been covered by a wooden platform, while a culvert channels the outlet under the platform at the contact between the RH PDC deposit and the conglomerate. Containment structures built to support the road and around the culvert seem unstable in the short term: landsliding affects the maar tuff and the RH PDC deposit on the west bank of the outlet headwall and the poorly maintained culvert may induce leakage (Figs. 5, 7A, B).

7. Concluding remarks

Lake Pavin illustrates the post-eruption evolution of maar lakes with emphasis on: (i) preserved lake terraces and outlet gorge landforms; (ii) distinct alluvial and mass-flow deposits in the fan down valley, and (iii) a series of ^{14}C dated deposits, although no direct dating of the early lake shores has been obtained. Since the eruption 6730 years ago, the Lake Pavin level change reflected a succession of four Stages and three intervals (Table 6, Fig. 11C).

1. Following the pristine north saddle at 1220 m termed Stage 0, the Stage 1 lake at 1215 m asl, i.e., +18 m above the current lake level, lasted about 5000 years until the 5-7th century CE. The Couze Pavin-Gelat valley was a palustrine basin between the 6-8th Century BCE and the 5-7th Century CE.
2. A slow drop of 14 m between the Stage 1 lake at 1215 m and the Stage 2 lake at 1201 m was initiated after the 7th century CE and may have lasted about a few hundred years. The meandering Couze Pavin was competing with the active lake outlet, which supplied material now intercalated in the fan Unit 2 and 3 deposits and pushed the river channel north of the Gelat valley.
3. The Stage 2 lake bench at c. 1201 m, about 4.35 m above the current lake level, reflects a pause in erosion and was probably reached after the 9th century.
4. A rapid drop of c. 4.35 m between the Stages 2 and 3 occurred well after the 9th century and prior to the 14th century, as recorded by the fan Unit 4 debris flows. This rapid incision did not cause any 'extreme' event, but may be due to heavy rainstorms and human impact enhancing runoff.
5. Stage 3 corresponds to the current lake level at c. 1197 m, which was reached before the early 18th Century. Lake level remained stable despite human impacts on the outlet, dam and access roads around 1860 and after 1950.
6. Downcutting exploited lithological contrasts at the lake dam. The composite succession of different materials in the outlet area resulted in some kind of stepwise lowering of Lake Pavin without apparent catastrophic breaching. The modern lake now coincides with the top of the indurated conglomerate.
7. Concern is raised by the long-term stability of the natural dam that impounds part of Lake Pavin. This issue requires additional geotechnical and mechanical investigations.

Declaration of competing interest

The authors declare that they have no known competing financial interests or personal relationships that could have appeared to influence the work reported in this paper.

Acknowledgements

This research project has benefited from the support of Laboratoire Magmas et Volcans through the research programme "Regional geology and volcanism". ^{14}C age analyses have been performed by the Laboratory LMC14 thanks to the ARTEMIS INSU program and L. Beck. We are indebted to the Town hall, in particular Mrs. Léger and Mr. Gay, Mayor of Besse for their logistical support. Laboratory and field analyses were conducted with the collaboration from C. Merceccia, N. Cluzel, T. Souriot, M. Benbakkar, C. Constantin, C. Fonquernie, L. Calabro and L. Grenet. T. Pilleyre contributed to the 3D print-out model and bibliographic search has been completed with S. Jouhannel's help.

Appendix A. Supplementary data

Supplementary data to this article can be found online at https://doi.org/10.1016/j.geomorph.2021.107663.

References

Aeschbach-Hertig, W., Kipfer, R., Hofer, M., Imboden, D.M., Wieler, R., Signer, P., 1996. Quantification of gas fluxes from the subcontinental mantle; the example of Laacher See, a maar lake in Germany. Geochim. Cosmochim. Acta 60, 1, 31–41.

Aeschbach-Hertig, W., Hofer, M., Schmid, M., Kipfer, R., Imboden, D.M., 2002. The physical structure and dynamics of a deep, meromictic crater alke (Lac Pavin, France). Hydrobiologia 487, 111–136.

Alberic, P., Jézéquel, D., Bergonzini, L., Chapron, E., Viollier, E., Massault, M., Michard, G., 2013. Carbon cycling and organic radiocarbon reservoir effect in a meromictic lake (Lac Pavin, Puy-de-Dôme, France). Radiocarbon 55, 2–3, 1029–1043.

Alvarado, G.E., Soto, G.J., Salani, F.M., Ruiz, P., Hurtado de Mendoza, L., 2011. The formation and evolution of Hule and Rio Cuarto maars, Costa Rica. J. Volcanol. Geotherm. Res. 201, 1–4 342–356. https://doi.org/10.1016/j.jvolgeores.2010.12.017.

Anzidei, M., Carapezza, M.L., Esposito, A., Giordano, G., Lelli, M., Tarchini, L., 2007. The Albano Maar Lake high resolution bathymetry and dissolved CO_2 budget (Colli Albani volcano, Italy): constrains to hazard evaluation. J. Volcanol. Geotherm. Res. 171, 34, 258–268.

Aramaki, S., Hayakawa, Y., Fujii, T., Nakamura, K., Fukuoka T., 1986. The October 1983 eruption of Miyakejima Volcano. J. Volcanol. Geotherm. Res. 29, 1–4, 203–229.

Aranda Gomez, J.J., Luhr, J.F., Pier, J.G., 1992. The La Brena - El Jaguee Maar Complex, Durango, Mexico; 1, Geological evolution. Bull. Volcanol. 54, 5, 93–404.

Baubron, J.C., Cantagrel, J.M., 1980. Les deux volcans des Monts Dore (Massif central français) : arguments chronologiques. CR Acad. Sci. Paris 290 (D, 1409–1412.

Boivin, P., Mergoil, J., 1993. Le Velay. Son volcanisme et les formations associées. Géol. Fr. 3 96 pp., carte à 1/100 000.

Boivin, P., Thouret, J.C., 2014. The volcanic Chaîne des Puys: a unique collection of simple and compound monogenetic edifices, Chapter 9. In: Fort, M., André, M.-F. (Eds.), Landscapes and Landforms of France. Springer, Heidelberg, pp. 81–91.

Boivin, P., Besson, J.-C., Ferry, P., Gourgaud, A., Miallier, D., Thouret, J.-C., Vernet, G., 2012. Le point sur l'éruption du Lac Pavin, il y a 7000 ans. Actes du colloque international « Lac Pavin et autres lacs méromictiques », Besse-St-Anastaise, 14–16 mai 2009. Rev. Sci. Nat. Auvergne 74–75, 45–55.

Boivin, P., Besson, J.C., Briot, D., Deniel, C., Gourgaud, A., Labazuy, P., Langlois, E., Larouzière, F.-D. de, Livet, M., Médard, E., Merciecca, C., Mergoil, J., Miallier, D., Morel, J.-M., Thouret, J.-C., Vernet, G., 2017. Volcanologie de la Chaîne des Puys. Carte au 1/25 000, Notice 200 pp. Parc Naturel Régional des Volcans d'Auvergne, Montlosier.

Bonelli, S., Brivois, O., Benahmed, N., 2007. Modélisation du renard hydraulique et interprétation de l'essai d'érosion de trou. Rev. Franç. Géotech. 118, 13–22.

Boule, M., 1896. Sur l'origine géologique des lacs d'Auvergne et du Velay. Bull. Soc. Géol. Fra. XXIV, 759.

Bourdier, J.-L., 1980. Contribution à l'étude volcanologique de deux secteurs d'intérêt géothermique dans le Mont Dore : le groupement holocène du Pavin et le massif du Sancy. Thèse (Unpubl., in French), Université de Clermont II, 180 p.

BRGM, 2007. Commune de Besse et Saint-Anastaise (63). Elaboration d'une carte d'aléa "mouvement de terrain" des flancs internes du Lac Pavin – Mise en place d'un réseau de suivi topographique. Report RP-53301-FR, 33 p., Orléans (in French).

BRGM, Renault, O., 2009. Evaluation préliminaire des conditions de stabilité des pentes du Lac Pavin. International Meeting "Lake Pavin and other meromictic lakes", Besse-St-Anastaise, 14–16 mai 2009. Service Aménagement et Risques naturels, DDE Puy de Dôme (Abstract).

BRGM, 2011. Étude complémentaire de la stabilité des flancs internes du cratère du Lac Pavin -63). Rapport final RP59980-FR, 31 p, Orléans (in French).

Bruyant, C., 1909. Le niveau du Pavin, *in:* Mélanges, 3è partie, Annales de la station limnologique de Besse, 203–205.

Büchel, G., 1993. Maars of the westEifel, Germany, *in:* Negendank, J.F.W., Zolitschka, B. (Eds.), Paleolimnology of European Maar Lakes, pp. 1–13. Lecture Notes in Earth Sciences 49, Springer Verlag, Berlin.

Büchel, G., Lorenz, V., 1993. Syn- and post-eruptive mechanism of the Alaskan Ukinrek mars in 1977, *in*: Negendank, J.F.W., Zolitschka, B. (Eds.), Paleolimnology of European Maar Lakes, pp. 15–60. Lecture Notes in Earth Sciences 49, Springer Verlag, Berlin.

Cabassi, J., Tassi, F., Vaselli, O., Fiebig, J., Nocentini, M., Capecchiacci, F., Rouwet, D., Bicocchi, G., 2013. Biogeochemical processes involving dissolved CO_2 and CH_4 at Albano, Averno, and Monticchio meromictic volcanic lakes (Central-Southern Italy). Bull. Volcanol. 75, 1, 683. https://doi.org/10.1007/s00445-012-0683-0.

Camus, G., de Goër de Herve, A., Kieffer, G., Mergoil, J., Vincent, P.-M., 1973. Mise au point sur le dynamisme et la chronologie des volcans holocènes de la région de Besse-en-Chandesse (Massif Central francais). CR Acad. Sci. Paris 277, 7, 629–632.

Camus, G., Michard, G., Olive, P., Boivin, P., Desgranges, P., Jézéquel, D., Meybeck, M., Peyrus, J.-C., Vinson, J.M., Viollier, E., Kornprobst, J., 1993. Risque d'éruption gazeuse carbonique en Auvergne. Bull. Soc. Géol. Fra. 164, 6, 767–781.

Capra, L., 2007. Volcanic natural dams: identification, stability, and secondary effects. Nat. Hazards 43, 45–61. https://doi.org/10.1007/s11069-006-9101-2.

Caracausi, A., Nicolosi, M., Nuccio, P.M., Favara, R., Paternoster, M., Rosciglione, A., 2013. Geochemical insight into differences in the physical structures and dynamics of two adjacent maar lakes at Mt. Vulture volcano (southern Italy). Geochem. Geophys. Geosyst. 14, 1411–1434. https://doi.org/10.1002/ggge.20111.

Chapron, E., Albéric, P., Jézéquel, D., Versteeg, W., Bourdier, J.-L., Sitbon, J., 2010. Multidisciplinary characterization of sedimentary processes in a recent maar (Lake Pavin, French Massif Central) and implication for natural hazards. Nat. Hazards Earth Syst. Sci. 10, 1815–1827. https://doi.org/10.5194/nhess-10-1815-2010.

Chapron, E., Ledoux, G., Simonneau, A., Albéric, P., St-Onge, G., Lajeunesse, P., Boivin, P., Desmet, M., 2012. New evidence of Holocene mass wasting events in recent volcanic lakes from the French Massif Central (Lakes Pavin, Montcineyre and Chauvet) and implications for natural hazards, *in:* Yamada, Y., Kawamura, K., Ikehara, K., Ogawa, Y., Urgeles, R., Mosher, D., Chaytor, J., Strasser, M. (Eds.), Submarine Mass Movements and Their Consequences, pp. 255–264. Advances in Natural and Technological Hazard Research vol. 31, Springer, doi::https://doi.org/10.1007/978-94-007-2162-3_23.

Chassiot, L., Chapron, E., Di Giovanni, C., Albéric, P., Lajeunesse, P., Lehours, A.-C., Meybeck, M., 2016a. Extreme events in the sedimentary record of maar Lake Pavin: implication for natural hazards assessment in the French Massif Central. Quat. Sci. Rev. 141, 9–25.

Chassiot, L., Chapron, E., Di Giovanni, C., Lajeunesse, P., Tachikawa, K., Garcia, M., Bard, E., 2016b. Historical seismicity of the Mont Dore volcanic province (Auvergne, France), unraveled by a regional lacustrine investigation: new insights about lake sensitivity to earthquakes. Sediment. Geol. 339, 134–150.

Chassiot L., Chapron, E., Miras, Y., Schwab, M.J., Albéric, P., Beauger, A., Anne- Lise Develle, A.-L., Arnaud, F., Lajeunesse, P. Zocatelli, R., Bernard, S., Lehours, A.-C., Jézéquel, D., 2016c. Lake Pavin paleolimnology and event stratigraphy, Chapter 23, pp. 381–406, *in*: Sime-Ngando, T. et al. (eds.), Lake Pavin, Springer Internat Publ, doi:https://doi.org/10.1007/978-3-319-39961-4_23.

Chassiot, L., Miras, Y., Chapron, E., Develle, A.-L., Arnaud, F., Motelica-Heino, M., Di Giovannia, C., 2018. A 7000-year environmental history and soil erosion record inferred from the deep sediments of Lake Pavin (Massif Central, France). Palaeogeogr. Palaeoclimatol. Palaeoecol. 497, 218–233. https://doi.org/10.1016/j.palaeo.2018.02.024.

Christenson, B., Németh, K., Rouwet, D., Tassi, F., Vandemeulebrouck, J., Varekamp, J.C., 2015. Volcanic lakes. In: Rouwet, D., Christenson, B., Tassi, F., Vandemeulebrouck, J. (Eds.), Volcanic Lakes. Springer-Verlag, Berlin - Heidelberg, pp. 1–20.

Cioni, R., Marini, L., Raco, B., 2006. The Lake Piccolo di Monticchio: fluids geochimistry and evaluation of the limnic eruption hazard, pp. 171–177 *in:* The Geology of Mount Vulture (C. Principe, Ed.), Consiglio Nazionale delle Ricerche, Regione Basilicata (in Italian).

Corwin, G., Forster, H.L., 1959. The 1957 explosive eruption on Iwo Jima, Volcano Islands. Am. J. Sci. 257, 161–171.

De Benedetti, A.A., Funiciello, R., Giordano, G., Diano, G., Caprilli, E., Paterne, M., 2008. Volcanology, history and myths of the Lake Albano maar (Colli Albani volcano, Italy). J. Volcanol. Geotherm. Res. 176, 3, 387–406. https://doi.org/10.1016/j.jvolgeores.2008.01.035.

De Goer de Herve, A., 2000. Description of a section behind the hotel and tourism building on the east slope of the lake platform (Pictures of this section by P. Lavina and A. Finizola). Archives of EAVUC, Clermont-Ferrand (Unpubl., in French) 2 p.

Delmelle, P., Bernard, A., 2000. Volcanic lakes. In: Sigurdsson, H., et al. (Eds.), Encyclopedia of Volcanoes, first ed. Academic Press, pp. 877–896.

Delmelle, P., Henley, R.W., Bernard, A., 2015. Volcano-related lakes, pp. 851–864, *in*: Sigurdsson, H. et al (eds.), Encyclopedia of Volcanoes, 2nd ed., Academic Press.

Douglas, J., 2003. Earthquake ground motion estimation using strong-motion records: a review of equations for the estimation of peak ground acceleration and response spectral ordinates. Earth-Sci. Rev. 61, 1–2 43-104. https://doi.org/10.1016/S0012-8252(02)00112-5.

Eusébio, A., Reynouard, J, 1926. Le lac Pavin, le Creux du Soucy : guide du Touriste et du Naturaliste. Bibliothèque municipale et universitaire de Clermont-Ferrand.

Fepuleai, A., Gale, S.J., Wales, N.A., McInerney, S.P.L., Lal, K.K., Alloway, B.V., 2018. Post-eruptive sedimentary processes in volcanic crater lakes: implications for deciphering the Samoan sedimentary record. J. Paleolimnol. 21. https://doi.org/10.1007/s10933-018-0035-y.

Fox, B.R.S., Wartho, J., Wilson, G.S., Lee, D.E., Nelson, F.E., Kaulfuss, U., 2015. Long-term evolution of an Oligocene/Miocene maar lake from Otago, New Zealand. Geochem. Geophys. Geosyst. 16, 1, 59–76.

Freundt, A., Strauch, W., Kutterolf, S., Schmincke, H.-U., 2007. Volcanogenic Tsunamis in Lakes: examples from Nicaragua and General Implications. Pure Appl. Geophys. 164, 527–545. https://doi.org/10.1007/s00024-006-0178-z.

Funiciello, R., Giordano, G., De Rita, D., 2003. The Albano maar lake (Colli Albani Volcano, Italy): recent volcanic activity and evidence of pre-Roman Age catastrophic lahar events. J. Volcanol. Geotherm. Res. 123, 1–2 43-61. https://doi.org/10.1016/S0377-0273(03)00027-1.

Gal, F., Gadalia, A., 2011. Soil gas measurements around the most recent volcanic system of metropolitan France (Lake Pavin, Massif Central). C.R. Geosci. Acad. Sci. 343, 43–54. https://doi.org/10.1016/j.crte.2010.11.008.

Gautié, 1867. Lettre S 104-6 et Rapport « Aménagement des eaux du lac Pavin », Ponts et Chaussées n°9, bordereau n°2. Archives départementales du Puy de Dôme (63), Clermont-Ferrand (Unpubl., in French).

Glangeaud, Ph., 1916. Le cratère-lac du Pavin et le volcan de Montchalm (Puy-de-Dôme). C.R. Acad. Sc. Paris 162, 428–430.

Glangeaud, Ph., Boule, M., 1925. Carte géologique de la France 1/80 000, feuille Brioude, 2è édition.

Graettinger, A.H., 2018. Trends in maar size and shape using the global Maar Volcano Location and Shape (MaarVLS) database. J. Volcanol. Geotherm. Res. 357, 1–13.

Graettinger, A.H., Valentine, G.A., 2017. Evidence for the relative depths and energies of phreatomagamtic explosions recorded in tephra rings. Bull. Volcanol. 79, 88. https://doi.org/10.1007/s00445-017—1177-x.

Henriet, J.-P., 2009. Geophysical reconnaissance of Lake Pavin 2002. International Meeting "Lake Pavin and other meromictic lakes", Abstract, Besse et St Anastaise, 14-16 May 2009.

Illies, H., 1959. Die Entstehungsgeschichte eines Maares in Südchile (Ein aktuogeologischer Beitrag zum Problem des Maar-Vulkanismus). Geol. Rundsch. 48, 232–247.

Jézéquel, D., Sarazin, G., Fonty, G., Tassin, B., 2008. Le Lac Pavin: le volcan, l'eau et la vie. Pour La Science, dossier n°58 « L'EAU, ATTENTION FRAGILE ! », janvier-mars 2008, pp. 52–59.

Jézéquel, D., Sarazin, G., Prévot, F., Viollier, E., Groleau, A., Michard, G., Agrinier, P., Albéric, P., Binet, S., Bergonzini, L., 2011. Bilan hydrique du lac Pavin. Rev. Sci. Nat. Auvergne. vols. 74-75. Le lac Pavin, Numéro spécial, pp. 67–90.

Jouhanneau, A., Antoine, P, Wong, B, 2001. Le lac de Nyos. Rapport de la mission Hydraulique Sans Frontières (HSF), pour estimer la stabilité actuelle du barrage naturel. Propositions de consolidation. 16 p + annexes (Unpub. Report, in French).

Juvigné, E., 1992. Approche de l'âge de deux cratères volcaniques lacustres d'Auvergne (France). CR Acad. Sci. Paris 314, 401–414.

Juvigné, E., Miallier, D., 2016. Distribution, tephrostratigraphy and chronostratigraphy of the widespread eruptive products of Pavin volcano. Chapter 8. In: Sime-Ngando, T., et al. (Eds.), Lake Pavin. Springer International Publishing, pp. 143–154 https://doi.org/10.1007/978-3-319-39961-4_8.

Kaulfuss, U., 2017. Crater stratigraphy and the post-eruptive evolution of Foulden Maar, southern New Zealand. N.Z. J. Geol. Geophys. https://doi.org/10.1080/00288306.2017.1365733.

Kienle, J., Kyle, P.R., Self, S., Motyka, R.J., Lorenz, V., 1980. Ukinrek maars, Alaska I. April 1977 Eruption sequence, petrology and tectonic setting. J. Volcanol. Geotherm. Res. 7, 11–31.

Kipfer, R., Aeschbach-Hertig, W., Baur, H., Hofer, M., Imboden, D.M., Signer, P., 1994. Injection of mantle type helium into Lake Van (Turkey): the clue for quantifying deep water renewal. Earth Planet. Sci. Lett. 125, 357–370.

Kling, G. W., Clark, M.A., Compton, H.R., Devine, J.D., Evans, W.C., Humphrey, A.M., Koenigsberg, E.J., Lockwood, J.P., Tuttle, M.L., Wagner, G.N., 1987. The 1986 Lake Nyos gas disaster in Cameroon, West Africa. Science 236, 4798, 169–75.

Kling, G.W., Evans, W.C., Tanyileke, G., Kusakabe, M., Ohba, T., Yoshida, Y., Hell, J.V., 2005. Degassing Lakes Nyos and Monoun: defusing certain disaster. Proc. Natl. Acad. Sci. U. S. A. 102, 14185–14190.

Kusukabe, M., 2017. Lake Nyos and Monoun gas disasters (Cameroon)- Limnic eruptions caused by excessive accumulation of magmatic CO_2 in crater lakes. Geochem. Monogr. Ser. 1, 1, 1–50. https://doi.org/10.5047/gems.2017.00101.0001.

Lavina, P., 1985. Le volcan du Sancy et le « Massif Adventif » (Massif des Monts Dore, Massif Central Français). Etudes volcanologiques et structurales. Thèse 3è cycle (Unpubl., in French), Université de Clermont II, 197 p.

Lavina, P, Del Rosso d'Hers, T, 2008. Le système volcanique holocène Montcineyre – Montchal – Pavin. Nouvelles stratigraphie, teprochronologies et datations, vers une ré-évaluation de l'aléa volcanotectonique en Auvergne. Abstract, 22è Réunion Annuelle Sciences de la Terre, Nancy, France.

Lavina, P., Del Rosso d'Hers, T., 2009. Le système volcanique du groupe Montchal-Pavin : nouvelle stratigraphie des formations volcano-sédimentaires et nouvelles datations, volcanologie dynamique, conséquences pour une évaluation des risques naturels. International meeting "Lake Pavin and other meromictic lakes", 14-16 May 2009, Abstracts and Programme, Besse et St Anastaise, France.

Lavrieux, M., Disnar, J.-R., Chapron, E., Bréheret, J.-G., Jacob, J., Miras, Y., Reyss, J.-L., Andrieu-Ponel, V., Arnaud, F., 2013. 6700 yr sedimentary record of climatic and anthropogenic signlas in Lake Aydat (French Massif Central). The Holocene 23, 9, 1317–1328. https://doi.org/10.1177/0959683613484616.

Lecoq, H., 1835. Description pittoresque de l'Auvergne. II. Le Mont-Dore et ses environs. J.-B. Baillière ed., Paris.

Legrand d'Aussy, 1794–1795. Voyage fait en 1787 et 1788 dans la ci-devant haute et basse Auvergne, aujourd'hui départements du Puys-de-Dômes, du Cantal et partie de celui de Haute Loire. Imprimerie des Sciences et arts, Paris, 3 volumes, 1491 pp.

Leyrit, H., Zylberman, W., Lutz, P., Jaillard, A., Lavina, P., 2016. Characterization of phreatomagmatic deposits from the eruption of the Pavin maar (France), Chapter 6, pp. 105–128, in: Sime-Ngando et al. (Eds.), Lake Pavin, History, geology, biogeochemistry and sedimentology of a deep meromictic maar lake. Springer.

Lockwood, J.P., Rubin, M., 1989. Origin and age of the Lake Nyos maar, Cameroon, *in*: Le Guern, F., Sigvaldason, G. (eds.), The Lake Nyos event and natural CO_2 degassing, I. J. Volcanol. Geotherm. Res. 39, 117–124.

Lockwood, J.P., Costa, J.E., Tuttle, M.L., Nni, J., Tebor, S.G., 1988. The potential for catastrophic dam failure at Lake Nyos maar, Cameroon. Bull. Volcanol. 50, 5, 340–349.

Lorenz, V., 1973. On the formation of Maars. Bull. Volcanol. 37, 2, 183–204.

Lorenz, V., 1986. On the growth of maars and diatremes and its relevance to the formation of tuff rings. Bull. Volcanol. 48, 265–274.

Lorenz, V., 2003. Maar-diatreme volcanoes, their formation and their setting in hard-rock or soft-rock environments. Geolines 15, 72–83.

Lorenz, V., 2007. Syn- and posteruptive hazards of maar-diatreme volcanoes. J. Volcanol. Geotherm. Res. 159, 285–312.

Macaire, J.J., Fourmont, A., Bréhéret, J.-G., Hinschberger, F., Trément, F., 2010. Quantitative analysis of climate versus human impact on sediment yield since the Lateglacial: the Sarlièvе palaeolake catchment (France). The Holocene 20, 4, 497–516.

Manville, V., 2004. Palaeohydraulic analysis of the 1953 Tangiwai lahar: the New Zealand worst volcanic disaster. Acta Vulcanol. 16, 137–152.

Manville, V., 2010. An overview of break-out floods from intra-caldera lakes. Glob. Planet. Chang. 70, 14–23. https://doi.org/10.1016/j.gloplacha.2009.11.004.

Manville, V., 2015. Volcano-hydrologic hazards from volcanic lakes. In: Rouwet, D., Christenson, B., Tassi, F., Vandemeleubrouck, J. (Eds.), Volcanic Lakes, Advances in Volcanology. Springer, pp. 21–72 https://doi.org/10.1007/978-3-642-36833-2_2 522 pp.

Manville, V., Cronin, S.J., 2007. Break-out lahar from New Zealand's Crater Lake. EOS Trans. AGU 88, 43, 441–442.

Marra, W.A., Braat, L., Baar, A.W., Kleinhans, M.G., 2014. Valley formation by groundwater seepage, pressurized groundwater outbursts and crater-lake overflow in flume experiments with implications for Mars. Icarus 232, 97–117. https://doi.org/10.1016/j.icarus.2013.12.026.

Martin, U., Németh, K., 2007. Blocky versus fluidal peperite textures developed in volcanic conduits, vents and crater lakes of phreatomagmatic volcanoes in Mio/Pliocene volcanic fields of Western Hungary. J. Volcanol. Geotherm. Res. 159, 1–3, 164–178.

Martin, U., Németh, K., Lorenz, V., White, J.D.L., 2007. Introduction: Maar-diatreme volcanism. J. Volcanol. Geotherm. Res. 159, 1–3, 1–3, doi:https://doi.org/10.1016/j.jvolgeores.2006.06.003.

Massey, C.I., Manville, V., Hancox, G.H., Keys, H.J., Lawrence, C., McSaveney, M., 2014. Outburst flood (lahar) triggered by retrogressive landsliding, 18 March 2007 at Mt Ruapehu, New Zealand—a successful early warning. Landslide 7, 303–315.

Meybeck, M., 2016a.Pavin, the birthplace of french limnology (1770– 2012), and its degassing controversy, pp. 3–27, *in*: Sime-Ngando T et al. (Eds.), Lake Pavin, History, Geology, Biogeochemistry, and Sedimentology of a Deep Meromictic Maar Lake. Springer.

Meybeck, M., 2016b. Pvin, a rich but fragmented history (200AD-2016), Chapter 2, pp. 29–52, *in*: Sime-Ngando, T et al. (Eds.), Lake Pavin, History, geology, biogeochemistry, and sedimentology of a deep meromictic lake. Springer.

Meybeck, M., Martin, J.M., Olive, P., 1975. Géochimie des eaux et des sédiments de quelques lacs volcaniques du Massif Central français. Internat. Verein. Theor. Angew. Limnol. 19, 2, 1150–1164.

Miallier, D., 2020. Variations récentes de niveau du lac Pavin : essai de mise en cohérence des différentes sources d'information. BSGF Earth Sci. Bull. 191, 4 doi:/10.1051/bsgf/2020006.

Müller, G., Veyl, G., 1957. The birth of Nilahue, a new maar type volcano at Rininahue, Chile. Abstract, 20th Internat. Geol. Congress, Section 1, pp. 375–396, Mexico City.

Németh, K., 2001. Long-term erosion-rate calculation from the Waipiata Volcanic Field (New Zealand) based on erosion remnants of scoria cones, tuff rings and maars. Géomorph. Relief Proc. Environ. 2, 137–152.

Németh, K., Cronin, S.J., 2007. Syn- and post-eruptive erosion, gully formation, and morphological evolution of a tephra ring in tropical climate erupted in 1913 in West Ambrym, Vanuatu. Geomorph. 86, 115–130.

Németh, K., Kereszturi, G., 2015. Monogenetic volcanism: personal views and discussion. Int. J. Earth Sci. 104, 8, 2131–2146.

Németh, K., Goth, K., Martin, U., Csillag, G., Suhr, P., 2008. Reconstructing paleoenvironment, eruption mechanism and paleomorphology of the Pliocene Pula maar, (Hungary). J. Volcanol. Geotherm. Res. 177, 2, 441–456.

Németh, K., Haller, M., Siebe, C. (eds.), 2011. From maars to scoria cones: the enigma of monogenetic volcanic fields. J. Volcanol. Geotherm. Res. 201, 1–4, 1–402.

Nomade, S., Pastre, J.-F., Nehlig, P., Guillou, H., Scao, V., Scaillet, S., 2014. Tephrochronology of the Mont-Dore volcanic massif (Massif central, France): new $^{40}Ar/^{39}Ar$ constraints on the late Pliocene and early Pleistocene activity. Bull. Volcanol. 76, 798. https://doi.org/10.1007/s00445-014-0798-6.

Olive, P., Boulègue, J., 2004. Etude biogéochimique d'un lac méromictique : le Lac Pavin, France. Géomorph. Relief Proc. Environ. 4, 305–316.

Ollier, C.D., 1967. Maars. Their characteristics, varieties and definition. Bull. Volcanol. 31, 45–73.

Omaly, N., 1968. Le Lac Pavin, historique et hydrobiology. Rev. Sc. Nat. Auvergne 34, 7–31.

Ort, M.H., Lefebvre, N.S., Neal, C.A., McConnell, V.S., Wohletz, K.H., 2018. Linking the Ukinrek 1977 maar-eruption observations to the tephra deposits: new insights into maar depositional processes. J. Volcanol. Geotherm. Res. 360, 36–60.

Palladino, D.M., Valentine, G.A., Sottili, G., Taddeucci, J., 2015. Maars to calderas: end-members on a spectrum of explosive volcanic depressions. Front. Earth Sci. 3, 36. https://doi.org/10.3389/feart.2015.00036.

Pasternak, G.B., Varekamp, J.C., 1997. Volcanic lake systematics: I. Physical constraints. Bull. Volcanol. 58, 528–538.

Pirrung, M., Büchel, G., Lorenz, V., Treutler, H.C., 2007. Post-eruptive development of the Ukinrek East maar since its eruption in 1977 AD in the periglacial area of southwest Alaska. Sediment. 55, 2, 305–334.

Provencher, L., Dubois, J.-M., 2008. Proposition d'une nomenclature géomorphologique du rivage lacustre et comparaison avec les rivages côtiers et fluviaux. La société Provancher d'Histoire Naturelle du Canada, Université de Sherbrooke, pp. 90–96.

Riguzzi, F., Pietrantonio, G., Baiocchi, V., Mazzoni, A., 2008. Water level and volume estimations of the Albano and Nemi lakes (central Italy). Ann. Geophys. 51, 4, 563–573.

Rondet, M., Martel, C., Bourdier, J.-L., 2019. The intermediate step in fractionation trends of mildly alkaline volcanic suites: an experimental insight from the Pavin trachyandesite (Massif Central, France). C.R. Geosci. 351, 525–529. https://doi.org/10.1016/j.crte.2019.07.003.

del Rosso-d'Hers, T., Lavina, P., Levi-Faict, T.W., 2009. Risques naturels volcaniques et périvolcaniques du système volcanique Montchal-Pavin-Montcineyre. International meeting "Lake Pavin and other meromictic lakes", 14–16 May 2009, Abstracts and Programme, Besse et St- Anastaise, France.

Volcanic lakes. In: Rouwet, D., Christenson, B.W., Tassi, F., Vandemeulebrouck, J. (Eds.), Advances in Volcanology. IAVCEI, Springer, pp. 1–20 533 pp.. ISBN 978-3-642-36832-5.

Rouwet, D., Chiodini, G., Ciuccarelli, C., Comastri, A., Costa, A., 2019. Lago Albano, the "anti-Nyos-type" lake: the past as a key for the future. J. Afr. Earth Sci. 150, 425–440.

Schaefer, L.N., Kennedy, B.M., Villeneuve, M.C., Cook, S.C.W., Jolly, A.D., Keys, H.J.R., Leonard, G.S., 2018. Stability assessment of the Crater Lake/Te Wai-a-moe overflow channel at Mt. Ruapehu (New Zealand), and implications for volcanic lake breakout triggers. J. Volcanol. Geotherm. Res. 358, 31–44.

Schettler, G., Schwab, M.J., Stebich, M., 2007. A 700-year record of climate change based on geochemical and palynological data from varved sediments (Lac Pavin, France). Chem. Geol. 240, 11–35.

Seib, N., Kley, J., Büchel, G., 2013. Identification of maars and similar volcanic landforms in the West Eifel Volcanic Field through image processing of DTM data: efficiency of different methods depending on preservation state. Int. J. Earth Sci. 102, 875–910 doi: 10.1007 / s00531-012-0829-5.

Self, S., Kienle, J., Huot, J.-P., 1980. Ukinrek Maars, Alaska, II. Deposits and formation of the 1977 craters. J. Volcanol. Geotherm. Res. 7, 39–65.
Sigurdsson, H., Devine, J.D., Tchoua, F.M., Presser, T.S., Pringle, M.K., Evans, W.C., 1987. Origin of the lethal gas burst from Lake Monoun, Cameroun. J. Volcanol. Geotherm. Res. 31, 1–16.
de Silva, S., Linsay, J.M., 2015. Primary volcanic landforms, pp. 273–297, *in*: Sigurdsson et al., eds., The Encyclopedia of Volcanoes, 2nd ed., Academic Press-Elsevier.
Sime-Ngando, T., Boivin, P., Chapron, E., Jézéquel, D., Meybeck, M., 2016. Lake Pavin. History, Geology, Biogeochemistry, and Sedimentology of a Deep Meromictic Lake. Springer Internat. Publ. Switzerland, p. 421.
Spicciarelli, R., Marchetto, A., 2019. The contrasting evolution of two volcanic lakes lying in the same caldera, Monticchio, Mt Vulture, Italy, inferred from literature records. Adv. Oceanogr. Limnol. 10, 7, 949. https://doi.org/10.4081/aiol.2019.7949.
Spicer, K.R., Mosbrucker, A.R., 2017. Bathymetric map and area/capacity table for Castle Lake, Washington. U.S. Geol. Survey Open-File Report, OF 2017–1145, 22 p.
Stebich, M., Bruchmann, C., Khulbe, T., Negendank, 2005. Vegetation history, human impact and climate change during the last 700 years recorded in annaually laminated sediments of Lac Pavin, France. Rev. Palaeobot. Palynol. 133, 115–133.
Suryo, I., Clarke, M.C.G., 1985. The occurrence and mitigation of volcanic hazards in Indonesia as exemplified at the Mount Merapi, Mount Kelut and Mount Galunggung volcanoes. Quat. J. Eng. Geol. 18, 79–98.
Tanyileke, G., Ntchantcho, R., Fantong, W.Y., Aka, F.T., Hell, J.V., 2019. 30 years of the Lakes Nyos and Monoun gas disasters: A scientific, technological, institutional and social adventure. J. Afr. Earth Sci. 150, 415–424.
Tassi, F., Rouwet, D., 2014. An overview of the structure, hazards, and methods of investigation of Nyos-type lakes from the geochemical perspective. J. Limnol. 73, 1, 55–70.
Tchindjang, M., 2018. Lake Nyos, a multirisk and vulnerability appraisal. Geosci. MDPI 8, 312. https://doi.org/10.3390/geosciences8090312.
Thouret, J.-C., Abdurachman, K.E., Bourdier, J.-L., Bronto, S., 1998. Origin, characteristics, and behaviour of subsequent lahars of the 1990 eruption at Kelud, East Java (Indonesia). Bull. Volcanol. 59, 460–480.
Thouret, J.-C., Boivin, P., Labazuy, P., Leclerc, A., 2016. Geology, geomorphology and slope instability of the Maar Lake Pavin (Auvergne, French Massif Central), chapter 9, pp. 155–174, in: Sime-Ngando, T. et al. (Eds.), Lake Pavin, Springer International Publishing, doi:https://doi.org/10.1007/978-3-319-39961-4_9.
Valentine, G.A., White, J.D.L., 2012. Revised conceptual model for maar-diatremes: subsurface processes, energetics, and eruptive products. Geol. 40, 1111–1114. https://doi.org/10.1130/G33411.1.
Valentine, G.A., White, J.D.L., Ross, P.S., Graettinger, A.H., Sonder, I., 2017. Updates to concepts on phreatomagmatic maar-diatremes and their pyroclastic deposits. Front. Earth Sci. 5, 68.
Varekamp, J.C., Pasternack, G., Rowe, G., 2000. Volcanic lake systematics. II. Chemical constraints. J. Volcanol. Geotherm. Res. 97, 161–179.
Vernet, G., 2013. La séquence sédimentaire des Gravanches / Gerzat : enregistrement d'événements « catastrophiques » à valeur chronologique en Limagne d'Auvergne (Massif central, France). Quaternaire 24, 2, 109–127.
Villemant, B., Caron, B., Thierry, P., Boivin, P., 2016. Magmatic evolution of Pavin's group of volcanoes: petrology, geochemistry and modeling of diferentiation processes. A preliminary study, Chapter 7. In: Sime-Ngando, T., et al. (Eds.), Lake Pavin. Springer Internat Publ, pp. 129–142 https://doi.org/10.1007/978-3-319-39961-4_7.
Vimont, E., 1889. Le lac Pavin est-il un cratère-lac ? Rev. Auvergne VI, 8–14.
Wagner, T.P., McKee, C.O., Kuduon, J., Kombua, R., 2003. Landslide-induced wave in a small volcanic lake: Kasu Tephra Cone, Papua New Guinea. Int. J. Earth Sci. 92, 405–406.
Wald, D.J., Worden, B.C., Quitoriano, V., Pankow, K.L., 2005. ShakeMap manual: technical manual, user's guide, and software guide. U.S. Geol. Survey 132 p.
Walsh, B., Jolly, A.D., Procter, J.N., 2016. Seismic analysis of the 13 October 2012 Te Maari, New Zealand, lake breakout lahar: insights into flow dynamics and the implications on mass flow monitoring. J. Volcanol. Geotherm. Res. 324, 144–155.
White, J.D.L., Ross, P.-S., 2011. Maar-diatreme volcanoes: a review. J. Volcanol. Geotherm. Res. 201, 1–29.
Wohletz, K., 1986. Explosive magma-water interactions: thermodynamics, explosions mechanisms, and field studies. Bull. Volcanol. 48, 245–264.
Wood, C.A., Kienle, J., 1990. Volcanoes of North America: United States and Canada. Cambridge Univ. Press, Cambridge 354 p.